A mixed finite element method with exactly divergence-free velocities for incompressible magnetohydrodynamics

Chen Greif [a], Dan Li [a], Dominik Schötzau [b,*], Xiaoxi Wei [b]

[a] *Department of Computer Science, University of British Columbia, Vancouver, BC, Canada V6T 1Z4*
[b] *Mathematics Department, University of British Columbia, Vancouver, BC, Canada V6T 1Z2*

ARTICLE INFO

ABSTRACT

We introduce and analyze a mixed finite element method for the numerical discretization of a stationary incompressible magnetohydrodynamics problem, in two and three dimensions. The velocity field is discretized using divergence-conforming Brezzi–Douglas–Marini (BDM) elements and the magnetic field is approximated by curl-conforming Nédélec elements. The H^1-continuity of the velocity field is enforced by a DG approach. A central feature of the method is that it produces exactly divergence-free velocity approximations, and captures the strongest magnetic singularities. We prove that the energy norm error is convergent in the mesh size in general Lipschitz polyhedra under minimal regularity assumptions, and derive nearly optimal a priori error estimates for the two-dimensional case. We present a comprehensive set of numerical experiments, which indicate optimal convergence of the proposed method for two-dimensional as well as three-dimensional problems.

1. Introduction

The field of magnetohydrodynamics (MHD) studies the behavior of electrically conducting fluids (such as liquid metals, plasmas, salt water, etc.) in electromagnetic fields [19,26,41]. The equations of electromagnetics and fluid dynamics are coupled through two fundamental effects: first, the motion of a conducting material in the presence of a magnetic field induces an electric current that modifies the existing electromagnetic field. Second, the current and the magnetic field generate the Lorentz force, which accelerates the fluid particles in the direction normal to both the magnetic field and the electric current. Our focus is on incompressible viscous fluids whose electric resistivity is non-negligible. The corresponding incompressible MHD model is a system of PDEs, where the Navier–Stokes equations are coupled with the Maxwell equations. Incompressible MHD has a number of technological and industrial applications such as metallurgical engineering, electromagnetic pumping, stirring of liquid metals, and measuring flow quantities based on induction; cf. [17,26].

We consider a standard form of the incompressible MHD equations as derived in [2, Section 2]; see also [25,26,31]. That is, we neglect phenomena involving high frequency as well as the convection current, and consider a non-polarizable, non-magnetizable and homogeneous medium. In addition, to make the curl–curl operator arising in the Maxwell equations amenable to discretization with Nédélec elements, we use the mixed formulation proposed in [46]. The governing equations are then of the form

$$-v\Delta\mathbf{u} + (\mathbf{u}\cdot\nabla)\mathbf{u} + \nabla p - \kappa(\nabla\times\mathbf{b})\times\mathbf{b} = \mathbf{f} \quad \text{in } \Omega, \tag{1.1a}$$

$$\kappa v_m\nabla\times(\nabla\times\mathbf{b}) + \nabla r - \kappa\nabla\times(\mathbf{u}\times\mathbf{b}) = \mathbf{g} \quad \text{in } \Omega, \tag{1.1b}$$

$$\nabla\cdot\mathbf{u} = 0 \quad \text{in } \Omega, \tag{1.1c}$$

$$\nabla\cdot\mathbf{b} = 0 \quad \text{in } \Omega. \tag{1.1d}$$

Here, $\mathbf{u}$ is the velocity, $\mathbf{b}$ the magnetic field, p the hydrodynamic pressure, and r is a Lagrange multiplier associated with the divergence constraint on the magnetic field $\mathbf{b}$. The functions $\mathbf{f}$ and $\mathbf{g}$ represent external force terms.

The above equations are characterized by three dimensionless parameters: the hydrodynamic Reynolds number $\text{Re} = v^{-1}$, the magnetic Reynolds number $\text{Rm} = v_m^{-1}$, and the coupling number κ. For further discussion of these parameters and their typical values, we refer the reader to [2,26,45]. We assume Ω is a bounded simply-connected Lipschitz polytope in $\mathbb{R}^d$ ($d = 2$ or 3), with a connected boundary $\partial\Omega$. In the two-dimensional case, the curl operator $\nabla\times$ applied to a vector $\mathbf{b} = (b_1, b_2)$ is defined as $\nabla\times\mathbf{b} = \frac{\partial b_2}{\partial x} - \frac{\partial b_1}{\partial y}$, while the curl of a scalar function r is determined by $\nabla\times r = \left(\frac{\partial r}{\partial y}, -\frac{\partial r}{\partial x}\right)$. Similarly, the cross product of two vectors $\mathbf{u} = (u_1, u_2)$ and $\mathbf{b} = (b_1, b_2)$ is given by $\mathbf{u}\times\mathbf{b} = u_1 b_2 - u_2 b_1$.

We consider the following homogeneous Dirichlet boundary conditions:

* Corresponding author.
E-mail addresses: greif@cs.ubc.ca (C. Greif), danli@cs.ubc.ca (D. Li), schoetzau@math.ubc.ca (D. Schötzau), weixiaoxi@math.ubc.ca (X. Wei).

$$\mathbf{u} = \mathbf{0} \quad \text{on } \partial\Omega, \tag{1.2a}$$

$$\mathbf{n} \times \mathbf{b} = \mathbf{0} \quad \text{on } \partial\Omega, \tag{1.2b}$$

$$r = 0 \quad \text{on } \partial\Omega \tag{1.2c}$$

with $\mathbf{n}$ being the unit outward normal on $\partial\Omega$. By taking the divergence of the magnetostatic equation (1.1b), we obtain the Poisson problem

$$\Delta r = \nabla \cdot \mathbf{g} \quad \text{in } \Omega, \quad r = 0 \quad \text{on } \partial\Omega. \tag{1.3}$$

Since $\mathbf{g}$ is typically divergence-free in physical applications, the multiplier r is typically zero and its primary purpose is to ensure stability; see [21, Section 3].

Various finite element methods for discretizing linear and non-linear MHD systems can be found in the literature. The magnetic field is often approximated by standard nodal (i.e., H^1-conforming) finite elements [2,25,29–31]. However, since the strongest magnetic singularities have regularity below H^1, straightforwardly applied nodal elements may fail to resolve them in non-convex polyhedral domains; see [15] and the references therein. A number of remedies have been proposed for electromagnetic problems, for example the weighted regularization approach in [16] or the approach in [5], whereby the divergence of the electric field is stabilized in $H^{-\alpha}$ with $\frac{1}{2} < \alpha < 1$. In [33], weighted regularization has been applied to a full incompressible MHD system.

In the mixed formulation of [46] the above mentioned difficulties associated with nodal elements are seamlessly avoided without the need for stabilizing the divergence. This approach amounts to introducing the Lagrange multiplier r, and yields the PDE system (1.1). As a result, it is possible to use curl-conforming Nédélec elements for approximating the magnetic field. For these elements, only tangential continuity is enforced across inter-elemental faces. This makes this approach feasible in situations of highly singular magnetic fields [34,40,42]. In the context of incompressible magnetohydrodynamics, a related mixed approach for the discretization of the magnetic unknowns was presented in [22].

We are interested in discretizations for incompressible MHD problems that are based on discontinuous Galerkin (DG) methods; see, e.g., the surveys [12,13,20], and the references therein. In [29], an interior penalty technique is applied to enforce continuity of the magnetic variable across domains with different electromagnetic properties, while nodal elements are employed in the interior. A full DG method is proposed in [36] for a linearized variant of the system (1.1), whereby all the variables are approximated in discontinuous finite element spaces, based on existing discretizations for the Oseen and Maxwell equations [9,10,35]. However, this approach requires a large number of degrees of freedom. Furthermore, a straightforward extension to the non-linear setting in a locally conservative fashion would require a post-processing procedure for smoothing the DG velocity approximations throughout the non-linear iteration [10].

In this paper we design a new finite element discretization, in an attempt to overcome the above mentioned difficulties. Instead of discontinuous elements for all unknowns, we use divergence-conforming Brezzi–Douglas–Marini (BDM) elements [7,11] for the approximation of the velocity field, and curl-conforming Nédélec elements [42] for the magnetic field, thereby substantially reducing the total number of the coupled degrees of freedom. The H^1-continuity of the velocity field is again enforced by a DG technique. A central feature of this discretization is that it yields exactly divergence-free velocity approximations, guaranteeing stability of the linearized system within each Picard iteration, without any other modifications. We note that divergence-conforming discretizations have been analyzed for the incompressible Navier–Stokes equations in [11]. For the magnetic approximation we have a discrete version of the desirable property (1.3) in contrast to the method presented in [36].

We prove well-posedness of our discretization, and show convergence under minimal regularity assumptions. Thus, our method captures the strongest magnetic singularities in non-convex polyhedra. Our numerical results clearly indicate optimal convergence rates in two and three dimensions, but we manage to show (nearly) optimal estimates only for the two-dimensional case. Specific details on this are given in Section 4 and are summarized in the conclusions in Section 6. We note that our method converges optimally for the linearized version of (1.1), as follows from the arguments in [36, Remark 3.3].

The rest of the paper is structured as follows. In Section 2 we state the well-posedness of the variational formulation of (1.1). Section 3 is devoted to the finite element discretization; the existence and uniqueness of approximate solutions are proved. In Section 4 we present and prove the main results—convergence and a priori error estimates. In Section 5 we present a series of numerical experiments validating the theoretical results. In Section 6 we end with some concluding remarks.

2. Variational formulation of an MHD problem

To write (1.1) in weak form, we denote by $(\cdot, \cdot)_\Omega$ the inner product in $L^2(\Omega)$ or $L^2(\Omega)^d$. Upon setting

$$\mathbf{V} = H_0^1(\Omega)^d = \left\{ \mathbf{u} \in H^1(\Omega)^d : \mathbf{u} = \mathbf{0} \text{ on } \partial\Omega \right\},$$

$$\mathbf{C} = H_0(\text{curl}; \Omega)$$
$$= \left\{ \mathbf{b} \in L^2(\Omega)^d : \nabla \times \mathbf{b} \in L^2(\Omega)^d, \mathbf{n} \times \mathbf{b} = \mathbf{0} \text{ on } \partial\Omega \right\},$$

$$Q = L_0^2(\Omega) = \left\{ p \in L^2(\Omega) : (p, 1)_\Omega = 0 \right\},$$

$$S = H_0^1(\Omega) = \left\{ r \in H^1(\Omega) : r = 0 \text{ on } \partial\Omega \right\},$$

the variational formulation of the incompressible MHD system (1.1) and (1.2) amounts to finding $(\mathbf{u}, \mathbf{b}, p, r) \in \mathbf{V} \times \mathbf{C} \times Q \times S$ such that

$$A(\mathbf{u}, \mathbf{v}) + O(\mathbf{u}, \mathbf{u}, \mathbf{v}) + C(\mathbf{b}, \mathbf{v}, \mathbf{b}) + B(\mathbf{v}, p) = (\mathbf{f}, \mathbf{v})_\Omega, \tag{2.1a}$$

$$M(\mathbf{b}, \mathbf{c}) - C(\mathbf{b}, \mathbf{u}, \mathbf{c}) + D(\mathbf{c}, r) = (\mathbf{g}, \mathbf{c})_\Omega, \tag{2.1b}$$

$$B(\mathbf{u}, q) = 0, \tag{2.1c}$$

$$D(\mathbf{b}, s) = 0 \tag{2.1d}$$

for all $(\mathbf{v}, \mathbf{c}, q, s) \in \mathbf{V} \times \mathbf{C} \times Q \times S$. The variational forms are given by

$$A(\mathbf{u}, \mathbf{v}) = \int_\Omega \nu \nabla \mathbf{u} : \nabla \mathbf{v} \, d\mathbf{x}, \quad O(\mathbf{w}, \mathbf{u}, \mathbf{v}) = \int_\Omega (\mathbf{w} \cdot \nabla) \mathbf{u} \cdot \mathbf{v} \, d\mathbf{x},$$

$$M(\mathbf{b}, \mathbf{c}) = \int_\Omega \kappa \nu_m (\nabla \times \mathbf{b}) \cdot (\nabla \times \mathbf{c}) \, d\mathbf{x},$$

$$C(\mathbf{d}, \mathbf{v}, \mathbf{b}) = \int_\Omega \kappa (\mathbf{v} \times \mathbf{d}) \cdot (\nabla \times \mathbf{b}) \, d\mathbf{x},$$

$$B(\mathbf{u}, q) = -\int_\Omega (\nabla \cdot \mathbf{u}) q \, d\mathbf{x}, \quad D(\mathbf{b}, s) = \int_\Omega \mathbf{b} \cdot \nabla s \, d\mathbf{x}.$$

To discuss the well-posedness of the mixed formulation (2.1), we introduce the product norms

$$\|(\mathbf{u}, \mathbf{b})\|_{V \times C} = \left(\nu \|\mathbf{u}\|_{H^1(\Omega)}^2 + \kappa \nu_m \|\mathbf{b}\|_{H(\text{curl}; \Omega)}^2 \right)^{\frac{1}{2}}, \quad (\mathbf{u}, \mathbf{b}) \in \mathbf{V} \times \mathbf{C},$$

$$\|(p, r)\|_{Q \times S} = \left(\frac{1}{\nu} \|p\|_{L^2(\Omega)}^2 + \frac{1}{\kappa \nu_m} \|r\|_{H^1(\Omega)}^2 \right)^{\frac{1}{2}}, \quad (p, r) \in Q \times S.$$

Here, the curl-norm is defined by

$$\|\mathbf{b}\|_{H(\text{curl}; \Omega)} = \left(\|\mathbf{b}\|_{L^2(\Omega)}^2 + \|\nabla \times \mathbf{b}\|_{L^2(\Omega)}^2 \right)^{\frac{1}{2}}.$$

Furthermore, we define the norm of the source terms by

$$|||(\mathbf{f}, \mathbf{g})||| = \left(\|\mathbf{f}\|_{L^2(\Omega)}^2 + \|\mathbf{g}\|_{L^2(\Omega)}^2 \right)^{\frac{1}{2}}.$$

Finally, we introduce the parameters

$$\bar{v} = \min\{v, \kappa v_m\},$$
$$\bar{\kappa} = \max\{1, \kappa\}.$$

The following result can be found in [46, Corollary 2.18 and Remark 2.14].

Theorem 2.1. *There is a constant $c_1 > 0$ only depending on Ω such that for small data with $c_1 \bar{\kappa} \bar{v}^{-2} |||(\mathbf{f}, \mathbf{g})||| < 1$, the MHD problem (2.1) has a unique solution $(\mathbf{u}, \mathbf{b}, p, r)$ in $\mathbf{V} \times \mathbf{C} \times Q \times S$. Moreover, we have the stability bound*

$$\|(\mathbf{u}, \mathbf{b})\|_{V \times C} \leqslant c_2 \frac{|||(\mathbf{f}, \mathbf{g})|||}{\bar{v}^{\frac{1}{2}}}$$

for a constant $c_2 > 0$ only depending on Ω.

3. Mixed finite element discretization

In this section, we introduce a mixed finite element method that employs divergence-conforming elements for the approximation of the velocity field and curl-conforming elements for the magnetic field. The H^1-continuity of the velocity is enforced by a DG technique.

3.1. Meshes and traces

We consider a family of regular and quasi-uniform triangulations $\mathcal{T}_h$ of mesh size h that partition the domain Ω into simplices $\{K\}$ (i.e., triangles for $d = 2$ and tetrahedra for $d = 3$). We denote by $\mathcal{F}_h$ the set of all edges ($d = 2$) or faces ($d = 3$) of $\mathcal{T}_h$. In the following, we generically refer to elements in $\mathcal{F}_h$ as faces. As usual, h_K denotes the diameter of the element K, and h_F is the diameter of the face F. Finally, we write $\mathbf{n}_K$ for the unit outward normal vector on the boundary ∂K of K.

The average and jump operators are defined as follows. Let $F = \partial K \cap \partial K'$ be an interior face shared by K and K', and let $\mathbf{x} \in F$. Let ϕ be a generic piecewise smooth function and denote by ϕ and ϕ' the traces of ϕ on F taken from within the interior of K and K', respectively. Then, we define the mean value $\{\{\cdot\}\}$ at $\mathbf{x} \in F$ as

$$\{\{\phi\}\} = \frac{1}{2}(\phi + \phi').$$

Furthermore, for a piecewise smooth vector-valued function ϕ, we define the jump:

$$[\![\boldsymbol{\phi}]\!] = \boldsymbol{\phi} \otimes \mathbf{n}_K + \boldsymbol{\phi}' \otimes \mathbf{n}_{K'},$$

where $\boldsymbol{\phi} \otimes \mathbf{n} = (\phi_i n_j)_{1 \leqslant i,j \leqslant d}$. On a boundary face $F = \partial K \cap \partial \Omega$, we set accordingly

$$\{\{\phi\}\} = \phi, \quad [\![\boldsymbol{\phi}]\!] = \boldsymbol{\phi} \otimes \mathbf{n}.$$

3.2. Mixed discretization

For $k \geqslant 1$, we wish to approximate the solution of (1.1) and (1.2) by finite element functions $(\mathbf{u}_h, \mathbf{b}_h, p_h, r_h) \in \mathbf{V}_h \times \mathbf{C}_h \times Q_h \times S_h$, where

$$\mathbf{V}_h = \left\{ \mathbf{u} \in H_0(\mathrm{div}; \Omega) : \mathbf{u}|_K \in \mathcal{P}_k(K)^d, \ K \in \mathcal{T}_h \right\},$$

$$\mathbf{C}_h = \left\{ \mathbf{b} \in H_0(\mathrm{curl}; \Omega) : \mathbf{b}|_K \in \mathcal{P}_{k-1}(K)^d \oplus R_k(K), \ K \in \mathcal{T}_h \right\},$$

$$Q_h = \left\{ p \in L_0^2(\Omega) : p|_K \in \mathcal{P}_{k-1}(K), \ K \in \mathcal{T}_h \right\},$$

$$S_h = \left\{ r \in H_0^1(\Omega) : r|_K \in \mathcal{P}_k(K), \ K \in \mathcal{T}_h \right\}. \tag{3.1}$$

Here, we denote by $H_0(\mathrm{div}; \Omega)$ the space

$$H_0(\mathrm{div}; \Omega) = \left\{ \mathbf{u} \in L^2(\Omega)^d : \nabla \cdot \mathbf{u} \in L^2(\Omega), \mathbf{u} \cdot \mathbf{n} = 0 \text{ on } \partial \Omega \right\}$$

by $\mathcal{P}_k(K)$ the space of polynomials of total degree at most k on element K, and by $R_k(K)$ the space of homogeneous vector polynomials of total degree k that are orthogonal to $\mathbf{x}$.

The space $\mathbf{V}_h$ is the divergence-conforming Brezzi–Douglas–Marini (BDM) space (see [7, Section III.3] for details); it has degrees of freedom specified for the normal components of functions along faces. The space $\mathbf{C}_h$ represents the first family of curl-conforming Nédélec elements (cf. [42, Chapter 5]); its degrees of freedom are defined for the tangential components of functions along faces. We notice that the finite element spaces $\mathbf{C}_h$, Q_h and S_h are conforming in $\mathbf{C}$, Q and S, respectively, while $\mathbf{V}_h$ is non-conforming in $\mathbf{V}$.

Now we consider the following finite element method: find $(\mathbf{u}_h, \mathbf{b}_h, p_h, r_h) \in \mathbf{V}_h \times \mathbf{C}_h \times Q_h \times S_h$ such that

$$A_h(\mathbf{u}_h, \mathbf{v}) + O_h(\mathbf{u}_h, \mathbf{u}_h, \mathbf{v}) + C(\mathbf{b}_h, \mathbf{v}, \mathbf{b}_h) + B(\mathbf{v}, p_h) = (\mathbf{f}, \mathbf{v})_\Omega, \tag{3.2a}$$

$$M(\mathbf{b}_h, \mathbf{c}) - C(\mathbf{b}_h, \mathbf{u}_h, \mathbf{c}) + D(\mathbf{c}, r_h) = (\mathbf{g}, \mathbf{c})_\Omega, \tag{3.2b}$$

$$B(\mathbf{u}_h, q) = 0, \tag{3.2c}$$

$$D(\mathbf{b}_h, s) = 0 \tag{3.2d}$$

for all $(\mathbf{v}, \mathbf{c}, q, s) \in \mathbf{V}_h \times \mathbf{C}_h \times Q_h \times S_h$.

The form A_h associated with the Laplacian is chosen as the standard interior penalty form [3,4]:

$$A_h(\mathbf{u}, \mathbf{v}) = \int_\Omega v \nabla_h \mathbf{u} : \nabla_h \mathbf{v} \, d\mathbf{x} - \sum_{F \in \mathcal{F}_h} \int_F \{\{v \nabla_h \mathbf{u}\}\} : [\![\mathbf{v}]\!] \, ds$$
$$- \sum_{F \in \mathcal{F}_h} \int_F \{\{v \nabla_h \mathbf{v}\}\} : [\![\mathbf{u}]\!] \, ds + \sum_{F \in \mathcal{F}_h} \frac{a_0 v}{h_F} \int_F [\![\mathbf{u}]\!] : [\![\mathbf{v}]\!] \, ds.$$

Here, ∇_h is the elementwise gradient operator, and $a_0 > 0$ is the interior penalty stabilization parameter; it has to be chosen larger than a threshold value which is independent of h, v, κ and v_m. For the convection form, we take the standard upwind form [39]:

$$O_h(\mathbf{w}, \mathbf{u}, \mathbf{v}) = \sum_{K \in \mathcal{T}_h} \int_K (\mathbf{w} \cdot \nabla) \mathbf{u} \cdot \mathbf{v} \, d\mathbf{x}$$
$$+ \sum_{K \in \mathcal{T}_h} \int_{\partial K \backslash \partial \Omega} \frac{1}{2} (\mathbf{w} \cdot \mathbf{n}_K - |\mathbf{w} \cdot \mathbf{n}_K|)(\mathbf{u}^e - \mathbf{u}) \cdot \mathbf{v} \, ds \tag{3.3}$$
$$- \int_{\partial \Omega} \frac{1}{2} (\mathbf{w} \cdot \mathbf{n} - |\mathbf{w} \cdot \mathbf{n}|) \mathbf{u} \cdot \mathbf{v} \, ds.$$

Here, $\mathbf{u}^e$ is the trace of $\mathbf{u}$ taken from the exterior of K. The remaining forms are the same as in the continuous case. Notice that due to the presence of the upwind terms the form $O_h(\mathbf{w}, \mathbf{u}, \mathbf{v})$ is not linear in the first argument; see also Lemma 4.6 and (3.6).

By choosing the divergence-conforming BDM elements as the approximating space for the velocity, the method gives exactly divergence-free velocity approximations; cf. [11]. Moreover, the Lagrange multiplier r_h vanishes identically for divergence-free source terms, thereby mimicking the continuous property in (1.3).

Proposition 3.1. *Let $(\mathbf{u}_h, \mathbf{b}_h, p_h, r_h)$ solve (3.2). Then we have:*

(i) $\nabla \cdot \mathbf{u}_h = 0$ *in Ω.*
(ii) *the Lagrange multiplier r_h is the solution of*

$$(\nabla r_h, \nabla s)_\Omega = (\mathbf{g}, \nabla s)_\Omega \quad \forall \, s \in S_h.$$

In particular, if $\mathbf{g}$ is solenoidal, then $r_h \equiv 0$.

Proof. To prove item (i), we proceed as in [11]. We note that $\nabla \cdot \mathbf{u}_h$ has vanishing mean value on Ω, and is a discontinuous polynomial of degree $k - 1$. Thus, we have $\nabla \cdot \mathbf{u}_h \in Q_h$. Eq. (3.2c) then implies that $\nabla \cdot \mathbf{u}_h$ is orthogonal to all functions $q \in Q_h$. Therefore, it is equal to zero.

To prove item (ii), we take $\mathbf{c} = \nabla s$ in Eq. (3.2b) (noting that $\nabla S_h \subset \mathbf{C}_h$) and obtain

$$(\mathbf{g}, \nabla s)_\Omega = M(\mathbf{b}_h, \nabla s) - C(\mathbf{b}_h, \mathbf{u}_h, \nabla s) + D(\nabla s, r_h) = D(\nabla s, r_h).$$

Here, we have used the fact that $\nabla \times \nabla s = \mathbf{0}$. Therefore, r_h satisfies

$$(\nabla r_h, \nabla s)_\Omega = (\mathbf{g}, \nabla s)_\Omega \quad \forall \, s \in S_h.$$

Since $(\mathbf{g}, \nabla s)_\Omega = (\nabla \cdot \mathbf{g}, s)_\Omega$, we have $r_h \equiv 0$ provided that $\nabla \cdot \mathbf{g} = 0$. $\square$

For our analysis, it will be convenient to introduce the following product forms:

$$\mathcal{A}_h(\mathbf{u}, \mathbf{b}; \mathbf{v}, \mathbf{c}) = A_h(\mathbf{u}, \mathbf{v}) + M(\mathbf{b}, \mathbf{c}),$$

$$\mathcal{O}_h(\mathbf{w}, \mathbf{d}; \mathbf{u}, \mathbf{b}; \mathbf{v}, \mathbf{c}) = O_h(\mathbf{w}, \mathbf{u}, \mathbf{v}) + C(\mathbf{d}, \mathbf{v}, \mathbf{b}) - C(\mathbf{d}, \mathbf{u}, \mathbf{c}),$$

$$\mathcal{B}(\mathbf{u}, \mathbf{b}; q, s) = B(\mathbf{u}, q) + D(\mathbf{b}, s),$$

$$\mathcal{L}(\mathbf{v}, \mathbf{c}) = (\mathbf{f}, \mathbf{v})_\Omega + (\mathbf{g}, \mathbf{c})_\Omega.$$

Then, the mixed discretization (3.2) is equivalent to the following saddle-point system: find $(\mathbf{u}_h, \mathbf{b}_h, p_h, r_h) \in \mathbf{V}_h \times \mathbf{C}_h \times Q_h \times S_h$ such that

$$\mathcal{A}_h(\mathbf{u}_h, \mathbf{b}_h; \mathbf{v}, \mathbf{c}) + \mathcal{O}_h(\mathbf{u}_h, \mathbf{b}_h; \mathbf{u}_h, \mathbf{b}_h; \mathbf{v}, \mathbf{c}) + \mathcal{B}(\mathbf{v}, \mathbf{c}; p_h, r_h) = \mathcal{L}(\mathbf{v}, \mathbf{c}),$$
$$\mathcal{B}(\mathbf{u}_h, \mathbf{b}_h; q, s) = 0$$

for all $(\mathbf{v}, \mathbf{c}, q, s) \in \mathbf{V}_h \times \mathbf{C}_h \times Q_h \times S_h$.

3.3. Stability properties

To discuss the stability properties of the finite element formulation (3.2), we introduce the discrete H^1-norm for the hydrodynamic velocity:

$$\|\mathbf{u}\|_{1,h} = \left(\sum_{K \in \mathcal{T}_h} \|\nabla \mathbf{u}\|_{L^2(K)}^2 + \sum_{F \in \mathcal{F}_h} h_F^{-1} \|[\![\mathbf{u}]\!]\|_{L^2(F)}^2 \right)^{\frac{1}{2}}.$$

We further define

$$\|(\mathbf{u}, \mathbf{b})\|_{V_h \times C_h} = \left(v \|\mathbf{u}\|_{1,h}^2 + \kappa v_m \|\mathbf{b}\|_{H(\mathrm{curl};\Omega)}^2 \right)^{\frac{1}{2}}.$$

First, we note that the forms $\mathcal{A}_h$ and $\mathcal{B}$ are continuous over the finite element spaces:

$$|\mathcal{A}_h(\mathbf{u}, \mathbf{b}; \mathbf{v}, \mathbf{c})| \leqslant C_\mathcal{A} \|(\mathbf{u}, \mathbf{b})\|_{V_h \times C_h} \|(\mathbf{v}, \mathbf{c})\|_{V_h \times C_h}, \tag{3.4}$$

$$|\mathcal{B}(\mathbf{v}, \mathbf{c}; q, s)| \leqslant C_\mathcal{B} \|(\mathbf{v}, \mathbf{c})\|_{V_h \times C_h} \|(q, s)\|_{Q \times S} \tag{3.5}$$

for all $\mathbf{u}, \mathbf{v} \in \mathbf{V}_h$, $\mathbf{b}, \mathbf{c} \in \mathbf{C}_h$, $q \in Q_h$, $s \in S_h$, with constants $C_\mathcal{A}, C_\mathcal{B} > 0$ independent of h, v, κ and v_m.

Next, we introduce the following spaces of (discretely) divergence-free functions:

$$\mathbf{J}_h = \{\mathbf{u} \in \mathbf{V}_h : B(\mathbf{u}, q) = 0 \, \forall \, q \in Q_h\},$$
$$\mathbf{X}_h = \{\mathbf{b} \in \mathbf{C}_h : D(\mathbf{b}, s) = 0 \, \forall \, s \in S_h\}.$$

For the form $\mathcal{O}_h$, we then have the following continuity result: there exists a constant $C_\mathcal{O} > 0$ independent of h, v, κ and v_m such that, for any $\mathbf{w}_1, \mathbf{w}_2 \in \mathbf{V}_h$, $\mathbf{u}, \mathbf{v} \in \mathbf{V}_h$, $\mathbf{d}_1, \mathbf{d}_2 \in \mathbf{X}_h$, and $\mathbf{b}, \mathbf{c} \in \mathbf{C}_h$, we have

$$|\mathcal{O}_h(\mathbf{w}_1, \mathbf{d}_1; \mathbf{u}, \mathbf{b}; \mathbf{v}, \mathbf{c}) - \mathcal{O}_h(\mathbf{w}_2, \mathbf{d}_2; \mathbf{u}, \mathbf{b}; \mathbf{v}, \mathbf{c})|$$
$$\leqslant \frac{C_\mathcal{O} \bar{\kappa}}{\bar{v}^{\frac{3}{2}}} \|(\mathbf{w}_1 - \mathbf{w}_2, \mathbf{d}_1 - \mathbf{d}_2)\|_{V_h \times C_h} \|(\mathbf{u}, \mathbf{b})\|_{V_h \times C_h} \|(\mathbf{v}, \mathbf{c})\|_{V_h \times C_h}; \tag{3.6}$$

see also Proposition 4.8 for a more detailed discussion.

Furthermore, the following stability properties of $\mathcal{A}_h$ and $\mathcal{O}_h$ hold; cf. [4,9,34, Theorem 4.7], and the references therein:

$$\mathcal{A}_h(\mathbf{u}, \mathbf{b}; \mathbf{u}, \mathbf{b}) \geqslant C_C \|(\mathbf{u}, \mathbf{b})\|_{V_h \times C_h}^2 \quad \forall \, (\mathbf{u}, \mathbf{b}) \in \mathbf{V}_h \times \mathbf{X}_h, \tag{3.7}$$

$$\mathcal{O}_h(\mathbf{w}, \mathbf{d}; \mathbf{u}, \mathbf{b}; \mathbf{u}, \mathbf{b}) = O_h(\mathbf{w}, \mathbf{u}, \mathbf{u}) \geqslant 0 \quad \forall \, \mathbf{w} \in \mathbf{J}_h, \; \mathbf{u} \in \mathbf{V}_h, \; \mathbf{b}, \mathbf{d} \in \mathbf{C}_h \tag{3.8}$$

with a constant $C_C > 0$ independent of h, v, κ and v_m.

Finally, let us address the inf–sup stability of the forms B and D. For the form B we have the following result [32, Proposition 10]:

$$\inf_{q \in Q_h} \sup_{\mathbf{v} \in \mathbf{V}_h} \frac{B(\mathbf{v}, q)}{\|\mathbf{v}\|_{1,h} \|q\|_{L^2(\Omega)}} = \lambda_h \geqslant C > 0, \tag{3.9}$$

where C is independent of h, v, κ and v_m. Moreover, since $\nabla S_h \subset \mathbf{C}_h$, there holds [35, Lemma 5.3]:

$$\inf_{s \in S_h} \sup_{\mathbf{c} \in \mathbf{C}_h} \frac{D(\mathbf{c}, s)}{\|\mathbf{c}\|_{H(\mathrm{curl};\Omega)} \|s\|_{H^1(\Omega)}} = \mu_h \geqslant C > 0 \tag{3.10}$$

for a constant C independent of h, v, κ and v_m.

An immediate consequence of (3.9) and (3.10) is the following inf–sup condition for the product form $\mathcal{B}$:

$$\inf_{(q,s) \in Q_h \times S_h} \sup_{(\mathbf{v}, \mathbf{c}) \in \mathbf{V}_h \times \mathbf{C}_h} \frac{\mathcal{B}(\mathbf{v}, \mathbf{c}; q, s)}{\|(\mathbf{v}, \mathbf{c})\|_{V_h \times C_h} \|(q, s)\|_{Q \times S}} \geqslant C_S > 0, \tag{3.11}$$

where the stability constant C_S is independent of h, v, κ and v_m.

In Table 3.1, we show the discrete inf–sup constants λ_h in (3.9) for the velocity–pressure pair $\mathbf{V}_h \times Q_h$ defined in (3.1). We use the lowest order BDM elements on $\Omega = (-1, 1)^2$ and compute the discrete inf–sup constants λ_h for a sequence of successively refined uniform triangular meshes. The inf–sup constants are obtained by solving a generalized eigenvalue problem related to the matrix representation of the bilinear form B and the norms in (3.9); cf. [7, p. 75]. Table 3.1 illustrates that the discrete inf–sup constants are approaching a positive lower bound as the mesh is refined.

3.4. Existence and uniqueness of discrete solutions

In the following theorem, we state the unique solvability of the method (3.2) under a discrete version of the smallness assumption in Theorem 2.1. The proof of this result follows along the same lines as [46, Theorem 2.12], using the stability properties outlined in Section 3.3.

Theorem 3.2. *There is a constant $C_1 > 0$ independent of h, v, κ and v_m such that for small data with $C_1 \bar{\kappa} \bar{v}^{-2} |||(\mathbf{f}, \mathbf{g})||| < 1$, the mixed finite element discretization (3.2) has a unique solution $(\mathbf{u}_h, \mathbf{b}_h, p_h, r_h) \in \mathbf{V}_h \times \mathbf{C}_h \times Q_h \times S_h$. Moreover, there is a constant $C_2 > 0$ independent of h, v, κ and v_m such that*

Table 3.1
Discrete inf–sup constants for $\mathbf{V}_h \times Q_h$.

Dofs in $\mathbf{u}_h$/ p_h	112/32	416/128	1600/512	6272/ 2048	24,832/ 8192
λ_h	1.273e−1	1.251e−1	1.241e−1	1.236e−1	1.233e−1

$$\|(\mathbf{u}_h, \mathbf{b}_h)\|_{V_h \times C_h} \leqslant C_2 \frac{\||(\mathbf{f}, \mathbf{g})\||}{\bar{\nu}^{\frac{1}{2}}}.$$

The solution of (3.2) can be found by employing the following Picard-type iteration: given $\left(\mathbf{u}_h^{n-1}, \mathbf{b}_h^{n-1}\right) \in \mathbf{V}_h \times \mathbf{C}_h$, let $(\mathbf{u}_h^n, \mathbf{b}_h^n, p_h^n, r_h^n)$ in $\mathbf{V}_h \times \mathbf{C}_h \times Q_h \times S_h$ be the solution of the linearized Oseen-type problem

$$A_h(\mathbf{u}_h^n, \mathbf{v}) + O_h(\mathbf{u}_h^{n-1}, \mathbf{u}_h^n, \mathbf{v}) + C(\mathbf{b}_h^{n-1}, \mathbf{v}, \mathbf{b}_h^n) + B(\mathbf{v}, p_h^n) = (\mathbf{f}, \mathbf{v})_\Omega,$$

$$M(\mathbf{b}_h^n, \mathbf{c}) - C(\mathbf{b}_h^{n-1}, \mathbf{u}_h^n, \mathbf{c}) + D(\mathbf{c}, r_h^n) = (\mathbf{g}, \mathbf{c})_\Omega,$$

$$B(\mathbf{u}_h^n, q) = 0,$$

$$D(\mathbf{b}_h^n, s) = 0$$

for all $(\mathbf{v}, \mathbf{c}, q, s) \in \mathbf{V}_h \times \mathbf{C}_h \times Q_h \times S_h$.

Theorem 3.2 guarantees the convergence of the iterates $\{(\mathbf{u}_h^n, \mathbf{b}_h^n, p_h^n, r_h^n)\}_{n \geqslant 0}$ to the solution $(\mathbf{u}_h, \mathbf{b}_h, p_h, r_h)$ of (3.2) for any initial guess $\left(\mathbf{u}_h^0, \mathbf{b}_h^0\right) \in \mathbf{V}_h \times \mathbf{C}_h$ with exactly divergence-free $\mathbf{u}_h^0$, provided that the small data assumption in Theorem 3.2 is satisfied. However, the scheme is only linearly convergent, as we illustrate in Section 5.

Remark 3.3. A more efficient non-linear solver such as Newton's method can also be used for solving (3.2); see, e.g., [24,26,31]. When upwinding is not incorporated, Newton's method can be straightforwardly applied. However, when upwind terms are included, adapting the non-linear iteration to our discretization is more delicate, since it requires additional linearization of the convection form $O_h(\mathbf{w}, \mathbf{u}, \mathbf{v})$ in the first argument. This remains an item for future investigation.

4. Error analysis

In this section, we present the main results of this paper, namely the convergence of finite element approximations and a priori error estimates for the two-dimensional version of our MHD problem. We provide detailed proofs in Sections 4.2 through 4.5.

4.1. Main results

Our first result is a convergence result. To state it, we suppose the solution $(\mathbf{u}, \mathbf{b}, p, r)$ of (1.1) and (1.2) possesses the smoothness

$$(\mathbf{u}, p) \in H^{\sigma+1}(\Omega)^d \times H^\sigma(\Omega), \tag{4.1a}$$

$$(\mathbf{b}, \nabla \times \mathbf{b}, r) \in H^\tau(\Omega)^d \times H^\tau(\Omega)^d \times H^{\tau+1}(\Omega) \tag{4.1b}$$

for $\sigma, \tau > \frac{1}{2}$.

Remark 4.1. The regularity assumption (4.1b) is minimal in the sense that it is satisfied by the strongest singularities of the Maxwell operator in polyhedral domains; cf. [15,16]. Similarly, the regularity (4.1a) holds true for the strongest singularities of the Stokes operator in polyhedral domains; see [1,18]. In view of these results, we expect (4.1) to be the minimal smoothness of solutions to the MHD system (1.1) and (1.2) in general Lipschitz polyhedra. However, we do not have a full proof of this conjecture.

Theorem 4.2. Let $(\mathbf{u}, \mathbf{b}, p, r)$ and $(\mathbf{u}_h, \mathbf{b}_h, p_h, r_h)$ be the solutions of (1.1), (1.2) and (3.2), respectively, obtained on a sequence of quasi-uniform meshes $\{\mathcal{T}_h\}_{h>0}$ of mesh size h. Assume (4.1) and that $\bar{\kappa}\bar{\nu}^{-2}\||(\mathbf{f}, \mathbf{g})\||$ is sufficiently small. Then we have

$$\lim_{h \to 0} \|(\mathbf{u} - \mathbf{u}_h, \mathbf{b} - \mathbf{b}_h)\|_{V_h \times C_h} = 0, \quad \lim_{h \to 0} \|(p - p_h, r - r_h)\|_{Q \times S} = 0.$$

Theorem 4.2 guarantees that the method (3.2) gives correct solutions provided that the (minimal) smoothness assumption (4.1) is satisfied and the data is sufficiently small. In particular, it ensures convergence in situations where straightforwardly applied nodal elements for the approximation of $\mathbf{b}$ are not capable of correctly capturing the singular solution components.

Next, we present a priori error estimates for the two-dimensional version of the MHD problem (3.2).

Theorem 4.3. Let $\Omega \subset \mathbb{R}^2$ be a simply-connected Lipschitz polygon with a connected boundary $\partial\Omega$. Under the same assumption as in Theorem 4.2, we have the following error estimates for any $\varepsilon > 0$:

$$\|(\mathbf{u} - \mathbf{u}_h, \mathbf{b} - \mathbf{b}_h)\|_{V_h \times C_h}$$
$$\leqslant C_\varepsilon h^{\min\{\sigma, \tau, k\} - \varepsilon} \left(\nu^{\frac{1}{2}} \|\mathbf{u}\|_{H^{\sigma+1}(\Omega)} + (\kappa \nu_m)^{\frac{1}{2}} \|\mathbf{b}\|_{H^\tau(\Omega)} \right.$$
$$\left. + (\kappa \nu_m)^{\frac{1}{2}} \|\nabla \times \mathbf{b}\|_{H^\tau(\Omega)} \right)$$
$$+ C h^{\min\{\sigma, \tau, k\}} \left(\nu^{-\frac{1}{2}} \|p\|_{H^\sigma(\Omega)} + (\kappa \nu_m)^{-\frac{1}{2}} \|r\|_{H^{\tau+1}(\Omega)} \right)$$

and

$$\|(p - p_h, r - r_h)\|_{Q \times S}$$
$$\leqslant C_\varepsilon h^{\min\{\sigma, \tau, k\} - 2\varepsilon} \left(\nu^{\frac{1}{2}} \|\mathbf{u}\|_{H^{\sigma+1}(\Omega)} + (\kappa \nu_m)^{\frac{1}{2}} \|\mathbf{b}\|_{H^\tau(\Omega)} + (\kappa \nu_m)^{\frac{1}{2}} \|\nabla \times \mathbf{b}\|_{H^\tau(\Omega)} \right)$$
$$+ C_\varepsilon h^{\min\{\sigma, \tau, k\} - \varepsilon} \left(\nu^{-\frac{1}{2}} \|p\|_{H^\sigma(\Omega)} + (\kappa \nu_m)^{-\frac{1}{2}} \|r\|_{H^{\tau+1}(\Omega)} \right).$$

Here, the constants C and C_ε are independent of h, ν, κ and ν_m. While C_ε depends on ε, the constant C does not.

The convergence rates in Theorem 4.3 are optimal in the mesh size, up to a loss of $\mathcal{O}(h^\varepsilon)$ for ε arbitrarily small. This loss stems from the use of the Sobolev embedding of $H^1(\Omega)$ into $L^p(\Omega)$, for all $p \geqslant 1$, but not into $L^\infty(\Omega)$; cf. [27]. To bridge this gap, we use inverse estimates to establish the continuity of the non-linear coupling form; see the proof of Lemma 4.7. In addition, the constant C_ε might become unbounded as ε tends to zero. However, in our numerical experiments this constant is observed to stay bounded. In fact, we observe optimal rates of convergence in all our tests, for both smooth and non-smooth solutions. Full details are given in Section 5.

Remark 4.4. Our technique of proof is applicable to three-dimensional problems. However, since in three dimensions the Sobolev embeddings are more restrictive, the use of the inverse estimates leads to convergence rates that fall short half a power of h for the error in $\mathbf{u}$ and $\mathbf{b}$, and a full power of h for the error in p and r (i.e., Theorem 4.3 holds with $\varepsilon = \frac{1}{2}$). To see this, we carry out the proof of Theorem 4.3 simultaneously for $d = 2$ and $d = 3$. We emphasize, however, that in our numerical tests, *optimal* convergence rates are observed for three-dimensional problems with smooth solutions.

Remark 4.5. For the linearized variant of the MHD system (1.1), our method converges optimally in the mesh size h, as follows from [36, Remark 3.3]. That is, the estimates of Theorem 4.3 hold true without any loss, both in two and three dimensions. However, there we make stronger smoothness assumptions on the linearized magnetic field. Therefore, this optimality cannot be straightforwardly carried over to the non-linear setting.

The proofs of Theorems 4.2 and 4.3 are presented in the next four subsections.

4.2. Continuity

We begin by revisiting the continuity properties of the forms in a more general setting. To that end, we introduce the space

$$\mathbf{V}(h) = \mathbf{V} + \mathbf{V}_h$$

and endow it with the norm $\|\cdot\|_{1,h}$. We then make use of an auxiliary form $\widetilde{A}_h(\mathbf{u},\mathbf{v})$ constructed as in [10,47] via the use of suitable lifting operators. It is defined as

$$\widetilde{A}_h(\mathbf{u},\mathbf{v}) = \int_\Omega v(\nabla_h\mathbf{u}:\nabla_h\mathbf{v} - \underline{\mathcal{L}}(\mathbf{v}):\nabla_h\mathbf{u} - \underline{\mathcal{L}}(\mathbf{u}):\nabla_h\mathbf{v})\,d\mathbf{x}$$
$$+ \sum_{F\in\mathcal{F}_h}\frac{a_0 v}{h_F}\int_F [\![\mathbf{u}]\!]:[\![\mathbf{v}]\!]\,ds,$$

where $\underline{\mathcal{L}}:\mathbf{V}(h) \to \underline{\Sigma}_h = \left\{\underline{\sigma}\in L^2(\Omega)^{d\times d}:\underline{\sigma}|_K\in\mathcal{P}_k(K)^{d\times d},\ K\in\mathcal{T}_h\right\}$ is the lifting operator given by

$$\int_\Omega \underline{\mathcal{L}}(\mathbf{u}):\underline{\sigma}\,d\mathbf{x} = \sum_{F\in\mathcal{F}_h}\int_F \{\!\{\underline{\sigma}\}\!\}:[\![\mathbf{u}]\!]\,ds \quad \forall\underline{\sigma}\in\Sigma_h.$$

By construction, the form $\widetilde{A}_h(\mathbf{u},\mathbf{v})$ satisfies

$$\begin{aligned}\widetilde{A}_h(\mathbf{u},\mathbf{v}) &= A(\mathbf{u},\mathbf{v}) \quad \forall\,\mathbf{u},\mathbf{v}\in\mathbf{V},\\ \widetilde{A}_h(\mathbf{u},\mathbf{v}) &= A_h(\mathbf{u},\mathbf{v}) \quad \forall\,\mathbf{u},\mathbf{v}\in\mathbf{V}_h.\end{aligned} \tag{4.2}$$

Furthermore, using arguments similar to those in [10,47], the form $\widetilde{A}_h(\mathbf{u},\mathbf{v})$ can be shown to be bounded on $\mathbf{V}(h)\times\mathbf{V}(h)$. Then, by setting

$$\widetilde{\mathcal{A}}_h(\mathbf{u},\mathbf{b};\mathbf{v},\mathbf{c}) = \widetilde{A}_h(\mathbf{u},\mathbf{v}) + M(\mathbf{b},\mathbf{c}),$$

we readily obtain

$$|\widetilde{\mathcal{A}}_h(\mathbf{u},\mathbf{b};\mathbf{v},\mathbf{c})| \leqslant C\|(\mathbf{u},\mathbf{b})\|_{V_h\times C_h}\|(\mathbf{v},\mathbf{c})\|_{V_h\times C_h} \tag{4.3}$$

for $\mathbf{u},\mathbf{v}\in\mathbf{V}(h)$ and $\mathbf{b},\mathbf{c}\in\mathbf{C}$. Moreover, we have

$$|\mathcal{B}(\mathbf{v},\mathbf{c};q,s)| \leqslant C\|(\mathbf{v},\mathbf{c})\|_{V_h\times C_h}\|(q,s)\|_{Q\times S} \tag{4.4}$$

for $(\mathbf{v},\mathbf{c},q,s)\in\mathbf{V}(h)\times\mathbf{C}\times Q\times S$.

In (4.3) and (4.4) and in the following, we denote by C a generic (positive) constant that is independent of the mesh size h and the parameters v, κ and v_m.

Next, we state the continuity of the convection term. The proof of this result follows similarly to the ones in [37, Proposition 4.15] and [10, Proposition 4.2].

Lemma 4.6. *There holds:*

$$|O_h(\mathbf{w}_1,\mathbf{u},\mathbf{v}) - O_h(\mathbf{w}_2,\mathbf{u},\mathbf{v})| \leqslant C\|\mathbf{w}_1-\mathbf{w}_2\|_{1,h}\|\mathbf{u}\|_{1,h}\|\mathbf{v}\|_{1,h}$$

for all $\mathbf{w}_1$, $\mathbf{w}_2\in\mathbf{V}(h)$, and $\mathbf{u},\mathbf{v}\in\mathbf{V}(h)$.

In the sequel, we shall analyze the two- and three-dimensional cases simultaneously (see also Remark 4.4). To do so, we introduce the function $\ell(d)$ given by

$$\ell(d) = \begin{cases} h^{-\varepsilon}, & d=2,\\ h^{-\frac{1}{2}}, & d=3. \end{cases} \tag{4.5}$$

Here, $\varepsilon > 0$ is a fixed number. The function $\ell(d)$ will indicate the loss of convergence rates for both the two-dimensional and three-dimensional cases. We also denote by $C_d > 0$ a generic constant independent of h, v, κ and v_m, but dependent on the dimension d. In particular, for $d = 2$ it depends on ε and might be unbounded as $\varepsilon \to 0$.

By introducing the kernel

$$\mathbf{X} = \{\mathbf{b}\in\mathbf{C}: D(\mathbf{b},s)=0 \quad \forall\,s\in S\}, \tag{4.6}$$

we state and prove the continuity of the coupling form $C(\mathbf{d},\mathbf{u},\mathbf{c})$ for several cases.

Lemma 4.7. *There holds:*

(i) *for $\mathbf{d}\in\mathbf{X}\cup\mathbf{X}_h$, $\mathbf{u}\in\mathbf{V}_h$ and $\mathbf{c}\in\mathbf{C}$:*

$$|C(\mathbf{d},\mathbf{u},\mathbf{c})| \leqslant C\kappa\|\mathbf{d}\|_{H(\mathrm{curl};\Omega)}\|\mathbf{u}\|_{1,h}\|\mathbf{c}\|_{H(\mathrm{curl};\Omega)}.$$

(ii) *for $\mathbf{d}\in\mathbf{X}\cup\mathbf{X}_h$, $\mathbf{u}\in\mathbf{V}(h)$ and $\mathbf{c}\in\mathbf{C}_h$:*

$$|C(\mathbf{d},\mathbf{u},\mathbf{c})| \leqslant C\kappa\|\mathbf{d}\|_{H(\mathrm{curl};\Omega)}\|\mathbf{u}\|_{1,h}\|\mathbf{c}\|_{H(\mathrm{curl};\Omega)}.$$

(iii) *for $\mathbf{d}\in\mathbf{C}$, $\mathbf{u}\in\mathbf{V}$ and $\mathbf{c}\in\mathbf{C}_h$:*

$$|C(\mathbf{d},\mathbf{u},\mathbf{c})| \leqslant C_d\ell(d)\kappa\|\mathbf{d}\|_{L^2(\Omega)}\|\mathbf{u}\|_{H^1(\Omega)}\|\mathbf{c}\|_{H(\mathrm{curl};\Omega)}.$$

(iv) *for $\mathbf{d}\in\mathbf{C}$, $\mathbf{u}\in\mathbf{V}_h$ and $\mathbf{c}\in\mathbf{C}$:*

$$|C(\mathbf{d},\mathbf{u},\mathbf{c})| \leqslant C_d\ell(d)\kappa\|\mathbf{d}\|_{L^2(\Omega)}\|\mathbf{u}\|_{1,h}\|\mathbf{c}\|_{H(\mathrm{curl};\Omega)}.$$

Proof. We proceed in two steps.

Step 1. We first discuss preliminary results that will be used in the proof. From the Poincaré inequality in [34, Corollary 4.4], there holds

$$\|\mathbf{b}\|_{L^2(\Omega)} \leqslant C\|\nabla\times\mathbf{b}\|_{L^2(\Omega)} \quad \forall\,\mathbf{b}\in\mathbf{X}. \tag{4.7}$$

Next, we recall the inverse inequality (cf. [6, Lemma 4.5.3]): for any $u\in\mathcal{P}_k(K)$, there holds

$$\|u\|_{L^{n_1}(K)} \leqslant Ch_K^{d\left(\frac{1}{n_1}-\frac{1}{n_2}\right)}\|u\|_{L^{n_2}(K)} \quad \forall\,1\leqslant n_1,n_2\leqslant\infty. \tag{4.8}$$

Further, let $\mathbf{H}:\mathbf{X}_h\to\mathbf{X}$ be the Hodge operator that maps discretely divergence-free functions into exactly divergence-free functions in such a way that

$$\nabla\times\mathbf{Hd} = \nabla\times\mathbf{d}. \tag{4.9}$$

It satisfies the following approximation property (cf. [34, Lemma 4.5]): there exists $\tau > \frac{1}{2}$ such that

$$\|\mathbf{d}-\mathbf{Hd}\|_{L^2(\Omega)} \leqslant Ch^\tau\|\nabla\times\mathbf{d}\|_{L^2(\Omega)} \quad \forall\,\mathbf{d}\in\mathbf{X}_h. \tag{4.10}$$

Finally, we present the following Sobolev embeddings:

$$\|\mathbf{u}\|_{L^{m(d)}(\Omega)} \leqslant C_d\|\mathbf{u}\|_{H^1(\Omega)} \quad \forall\,\mathbf{u}\in H^1(\Omega)^d, \tag{4.11a}$$

$$\|\mathbf{u}\|_{L^{m(d)}(\Omega)} \leqslant C_d\|\mathbf{u}\|_{1,h} \quad \forall\,\mathbf{u}\in\mathbf{V}(h), \tag{4.11b}$$

$$\|\mathbf{d}\|_{L^3(\Omega)} \leqslant C\|\mathbf{d}\|_{H(\mathrm{curl};\Omega)} \quad \forall\,\mathbf{d}\in\mathbf{X}. \tag{4.11c}$$

Here, $m(2) = 2/\varepsilon$ and $m(3) = 6$. The embedding (4.11a) is a standard result, while the embedding (4.11b) follows similarly to [28,38]. The inequality in (4.11c) follows from [1, Proposition 3.7].

Step 2. We are now ready to prove the bounds in the lemma. The proof of inequality (i) can be found in [46, Proposition 3.2].

To establish the second inequality, we follow [46, Lemma 2.6] and first show it for $\mathbf{d}\in\mathbf{X}$, $\mathbf{u}\in\mathbf{V}(h)$ and $\mathbf{c}\in\mathbf{C}_h$. This is done by applying Hölder's inequality and the Sobolev embeddings (4.11b) and (4.11c). We obtain

$$\begin{aligned}|C(\mathbf{d},\mathbf{u},\mathbf{c})| &\leqslant \kappa\|\mathbf{d}\|_{L^3(\Omega)}\|\mathbf{u}\|_{L^6(\Omega)}\|\nabla\times\mathbf{c}\|_{L^2(\Omega)}\\ &\leqslant C\kappa\|\mathbf{d}\|_{H(\mathrm{curl};\Omega)}\|\mathbf{u}\|_{1,h}\|\mathbf{c}\|_{H(\mathrm{curl};\Omega)}.\end{aligned} \tag{4.12}$$

Second, if $\mathbf{d}\in\mathbf{X}_h$, we decompose it into

$$\mathbf{d} = (\mathbf{d}-\mathbf{Hd}) + \mathbf{Hd},$$

where $\mathbf{H}$ is the Hodge operator in (4.9). We then rewrite $C(\mathbf{d},\mathbf{u},\mathbf{c})$ as

$$C(\mathbf{d},\mathbf{u},\mathbf{c}) = C(\mathbf{d}-\mathbf{Hd},\mathbf{u},\mathbf{c}) + C(\mathbf{Hd},\mathbf{u},\mathbf{c}). \tag{4.13}$$

Because $\mathbf{Hd}\in\mathbf{X}$, we can apply the previous argument (4.12), and bound the last term of (4.13) by

$$\begin{aligned}|C(\mathbf{Hd},\mathbf{u},\mathbf{c})| &\leqslant C\kappa\|\mathbf{Hd}\|_{H(\mathrm{curl};\Omega)}\|\mathbf{u}\|_{1,h}\|\mathbf{c}\|_{H(\mathrm{curl};\Omega)}\\ &\leqslant C\kappa\|\mathbf{d}\|_{H(\mathrm{curl};\Omega)}\|\mathbf{u}\|_{1,h}\|\mathbf{c}\|_{H(\mathrm{curl};\Omega)}.\end{aligned} \tag{4.14}$$

In (4.14), we have used the Poincaré inequality (4.7) and property (4.9) of the Hodge operator.

For the first term on the right-hand side of (4.13), we obtain from Hölder's inequality, the Sobolev embedding (4.11b) and the approximation property (4.10) that

$$|C(\mathbf{d} - \mathbf{Hd}, \mathbf{u}, \mathbf{c})| \leqslant \kappa \|\mathbf{d} - \mathbf{Hd}\|_{L^2(\Omega)} \|\mathbf{u}\|_{L^6(\Omega)} \|\nabla \times \mathbf{c}\|_{L^3(\Omega)}$$
$$\leqslant C\kappa h^\tau \|\nabla \times \mathbf{d}\|_{L^2(\Omega)} \|\mathbf{u}\|_{1,h} \|\nabla \times \mathbf{c}\|_{L^3(\Omega)}$$

for $\tau > \frac{1}{2}$. Finally, we apply the inverse estimate (4.8) to achieve

$$|C(\mathbf{d} - \mathbf{Hd}, \mathbf{u}, \mathbf{c})| \leqslant C\kappa \|\mathbf{d}\|_{H(\mathrm{curl};\Omega)} \|\mathbf{u}\|_{1,h} \|\nabla \times \mathbf{c}\|_{L^2(\Omega)} \quad (4.15)$$

for both $d = 2$ and $d = 3$. Referring to (4.13)–(4.15) proves the assertion of item (ii).

To verify item (iii), we define $m^*(d)$ such that

$$\frac{1}{m(d)} + \frac{1}{m^*(d)} = \frac{1}{2}.$$

Then we apply Hölder's inequality, the Sobolev embedding (4.11a) and the inverse estimate (4.8) to conclude that

$$|C(\mathbf{d}, \mathbf{u}, \mathbf{c})| \leqslant \kappa \|\mathbf{d}\|_{L^2(\Omega)} \|\mathbf{u}\|_{L^{m(d)}(\Omega)} \|\nabla \times \mathbf{c}\|_{L^{m^*(d)}(\Omega)}$$
$$\leqslant C_d \kappa \|\mathbf{d}\|_{L^2(\Omega)} \|\mathbf{u}\|_{H^1(\Omega)} \ell(d) \|\nabla \times \mathbf{c}\|_{L^2(\Omega)}.$$

The proof of item (iv) is similar to that of item (iii):

$$|C(\mathbf{d}, \mathbf{u}, \mathbf{c})| \leqslant \kappa \|\mathbf{d}\|_{L^2(\Omega)} \|\mathbf{u}\|_{L^\infty(\Omega)} \|\nabla \times \mathbf{c}\|_{L^2(\Omega)}$$
$$\leqslant C_d \kappa \|\mathbf{d}\|_{L^2(\Omega)} \ell(d) \|\mathbf{u}\|_{L^{m(d)}(\Omega)} \|\mathbf{c}\|_{H(\mathrm{curl};\Omega)}.$$

Applying (4.11b) finishes the proof. □

As an immediate consequence of Lemmas 4.6 and 4.7, the form $\mathcal{O}_h$ satisfies the following continuity properties.

Proposition 4.8. *There is a constant $C_\mathcal{O} > 0$ independent of h, v, κ and v_m such that there holds:*

(i) *for* $\mathbf{w}_1, \mathbf{w}_2 \in \mathbf{V}(h)$, $\mathbf{d}_1$, $\mathbf{d}_2 \in \mathbf{X} \cup \mathbf{X}_h$, $(\mathbf{u}, \mathbf{b}) \in \mathbf{V}(h) \times \mathbf{C}$, *and* $(\mathbf{v}, \mathbf{c}) \in \mathbf{V}_h \times \mathbf{C}_h$:

$$|\mathcal{O}_h(\mathbf{w}_1, \mathbf{d}_1; \mathbf{u}, \mathbf{b}; \mathbf{v}, \mathbf{c}) - \mathcal{O}_h(\mathbf{w}_2, \mathbf{d}_2; \mathbf{u}, \mathbf{b}; \mathbf{v}, \mathbf{c})|$$
$$\leqslant \frac{C_\mathcal{O} \bar\kappa}{\bar{v}^{\frac{3}{2}}} \|(\mathbf{w}_1 - \mathbf{w}_2, \mathbf{d}_1 - \mathbf{d}_2)\|_{V_h \times C_h} \|(\mathbf{u}, \mathbf{b})\|_{V_h \times C_h} \|(\mathbf{v}, \mathbf{c})\|_{V_h \times C_h}.$$

(ii) *for* $\mathbf{w}_1, \mathbf{w}_2 \in \mathbf{V}(h)$, $\mathbf{d}_1, \mathbf{d}_2 \in \mathbf{C}$, $(\mathbf{u}, \mathbf{b}) \in \mathbf{V} \times \mathbf{C}$, *and* $(\mathbf{v}, \mathbf{c}) \in \mathbf{V}_h \times \mathbf{C}_h$:

$$|\mathcal{O}_h(\mathbf{w}_1, \mathbf{d}_1; \mathbf{u}, \mathbf{b}; \mathbf{v}, \mathbf{c}) - \mathcal{O}_h(\mathbf{w}_2, \mathbf{d}_2; \mathbf{u}, \mathbf{b}; \mathbf{v}, \mathbf{c})|$$
$$\leqslant C_d \ell(d) \frac{C_\mathcal{O} \bar\kappa}{\bar{v}^{\frac{3}{2}}} \|(\mathbf{w}_1 - \mathbf{w}_2, \mathbf{d}_1 - \mathbf{d}_2)\|_{V_h \times C_h} \|(\mathbf{u}, \mathbf{b})\|_{V \times C} \|(\mathbf{v}, \mathbf{c})\|_{V_h \times C_h}.$$

4.3. Preliminary error estimates

In this subsection, we present two lemmas for estimating the errors. Let $(\mathbf{u}, \mathbf{b}, p, r)$ and $(\mathbf{u}_h, \mathbf{b}_h, p_h, r_h)$ be the solutions of (1.1), (1.2) and (3.2), respectively.

We begin by defining the residual

$$\mathcal{R}_A(\mathbf{v}) = \widetilde{A}_h(\mathbf{u}, \mathbf{v}) + O_h(\mathbf{u}, \mathbf{u}, \mathbf{v}) + C(\mathbf{b}, \mathbf{v}, \mathbf{b}) + B(\mathbf{v}, p) - (\mathbf{f}, \mathbf{v})_\Omega \quad (4.16)$$

for any $\mathbf{v} \in \mathbf{V}_h$. It measures how well the exact solution satisfies the finite element formulation expressed in terms of the auxiliary form $\widetilde{A}_h$ in (4.2). We have the following upper bound for the residual (cf. [47]):

$$\mathcal{R}_A(\mathbf{v}) \leqslant v^{\frac{1}{2}} \|\mathbf{v}\|_{1,h} \mathcal{E}(\mathbf{u}) \quad \text{with } \mathcal{E}(\mathbf{u}) \leqslant Ch^{\min\{\sigma, k\}} v^{\frac{1}{2}} \|\mathbf{u}\|_{H^{\sigma+1}(\Omega)}. \quad (4.17)$$

In the following, we shall denote the errors by

$$\mathbf{e_u} = \mathbf{u} - \mathbf{u}_h, \quad \mathbf{e_b} = \mathbf{b} - \mathbf{b}_h, \quad e_p = p - p_h, \quad e_r = r - r_h.$$

We shall also decompose the errors into

$$\begin{aligned}
\mathbf{e_u} &= \boldsymbol{\eta}_\mathbf{u} + \boldsymbol{\xi}_\mathbf{u} = (\mathbf{u} - \mathbf{v}) + (\mathbf{v} - \mathbf{u}_h), \\
\mathbf{e_b} &= \boldsymbol{\eta}_\mathbf{b} + \boldsymbol{\xi}_\mathbf{b} = (\mathbf{b} - \mathbf{c}) + (\mathbf{c} - \mathbf{b}_h), \\
e_p &= \eta_p + \xi_p = (p - q) + (q - p_h), \\
e_r &= \eta_r + \xi_r = (r - s) + (s - r_h)
\end{aligned} \quad (4.18)$$

for a discrete function $(\mathbf{v}, \mathbf{c}, q, s) \in \mathbf{V}_h \times \mathbf{C}_h \times Q_h \times S_h$ to be specified later.

Lemma 4.9. *Assume that*

$$\max\{c_2, C_2\} \frac{C_\mathcal{O}}{C_C} \frac{\bar\kappa \||(\mathbf{f}, \mathbf{g})|\|}{\bar{v}^2} < \frac{1}{2}. \quad (4.19)$$

Then there holds

$$\|(\mathbf{u} - \mathbf{u}_h, \mathbf{b} - \mathbf{b}_h)\|_{V_h \times C_h} \leqslant C_d \ell(d) \inf_{(\mathbf{v}, \mathbf{c}) \in \mathbf{V}_h \times \mathbf{C}_h} \|(\mathbf{u} - \mathbf{v}, \mathbf{b} - \mathbf{c})\|_{V_h \times C_h}$$
$$+ C \left(\mathcal{E}(\mathbf{u}) + \inf_{(q,s) \in Q_h \times S_h} \|(p - q, r - s)\|_{Q \times S} \right).$$

Proof. We proceed in two steps.

Step 1. In the error decomposition (4.18), we first consider $(\mathbf{v}, \mathbf{c}) \in \mathbf{J}_h \times \mathbf{X}_h$. Clearly, we also have $(\boldsymbol{\xi}_\mathbf{u}, \boldsymbol{\xi}_\mathbf{b}) \in \mathbf{J}_h \times \mathbf{X}_h$. In view of the residual defined in Eq. (4.16), we obtain

$$\begin{aligned}
\mathcal{R}_A(\boldsymbol{\xi}_\mathbf{u}) &= \widetilde{A}_h(\mathbf{e_u}, \mathbf{e_b}; \boldsymbol{\xi}_\mathbf{u}, \boldsymbol{\xi}_\mathbf{b}) + \mathcal{O}_h(\mathbf{u}, \mathbf{b}; \mathbf{u}, \mathbf{b}; \boldsymbol{\xi}_\mathbf{u}, \boldsymbol{\xi}_\mathbf{b}) \\
&\quad - \mathcal{O}_h(\mathbf{u}_h, \mathbf{b}_h; \mathbf{u}_h, \mathbf{b}_h; \boldsymbol{\xi}_\mathbf{u}, \boldsymbol{\xi}_\mathbf{b}) + \mathcal{B}(\boldsymbol{\xi}_\mathbf{u}, \boldsymbol{\xi}_\mathbf{b}; e_p, e_r) \\
&= \widetilde{A}_h(\mathbf{e_u}, \mathbf{e_b}; \boldsymbol{\xi}_\mathbf{u}, \boldsymbol{\xi}_\mathbf{b}) + \mathcal{O}_h(\mathbf{u}, \mathbf{b}; \mathbf{u}, \mathbf{b}; \boldsymbol{\xi}_\mathbf{u}, \boldsymbol{\xi}_\mathbf{b}) \\
&\quad - \mathcal{O}_h(\mathbf{u}_h, \mathbf{b}_h; \mathbf{u}, \mathbf{b}; \boldsymbol{\xi}_\mathbf{u}, \boldsymbol{\xi}_\mathbf{b}) + \mathcal{O}_h(\mathbf{u}_h, \mathbf{b}_h; \mathbf{e_u}, \mathbf{e_b}; \boldsymbol{\xi}_\mathbf{u}, \boldsymbol{\xi}_\mathbf{b}) \\
&\quad + \mathcal{B}(\boldsymbol{\xi}_\mathbf{u}, \boldsymbol{\xi}_\mathbf{b}; e_p, e_r).
\end{aligned}$$

Because $\mathbf{u}_h \in \mathbf{J}_h$ (see Proposition 3.1), the stability of $\mathcal{O}_h$ in (3.8) guarantees that

$$\mathcal{O}_h(\mathbf{u}_h, \mathbf{b}_h; \boldsymbol{\xi}_\mathbf{u}, \boldsymbol{\xi}_\mathbf{b}; \boldsymbol{\xi}_\mathbf{u}, \boldsymbol{\xi}_\mathbf{b}) \geqslant 0.$$

Therefore, we have

$$\begin{aligned}
&\widetilde{A}_h(\boldsymbol{\xi}_\mathbf{u}, \boldsymbol{\xi}_\mathbf{b}; \boldsymbol{\xi}_\mathbf{u}, \boldsymbol{\xi}_\mathbf{b}) + \mathcal{O}_h(\mathbf{v}, \mathbf{c}; \mathbf{u}, \mathbf{b}; \boldsymbol{\xi}_\mathbf{u}, \boldsymbol{\xi}_\mathbf{b}) \\
&\quad - \mathcal{O}_h(\mathbf{u}_h, \mathbf{b}_h; \mathbf{u}, \mathbf{b}; \boldsymbol{\xi}_\mathbf{u}, \boldsymbol{\xi}_\mathbf{b}) \\
&\leqslant \mathcal{R}_A(\boldsymbol{\xi}_\mathbf{u}) - \widetilde{A}_h(\boldsymbol{\eta}_\mathbf{u}, \boldsymbol{\eta}_\mathbf{b}; \boldsymbol{\xi}_\mathbf{u}, \boldsymbol{\xi}_\mathbf{b}) - \mathcal{B}(\boldsymbol{\xi}_\mathbf{u}, \boldsymbol{\xi}_\mathbf{b}; e_p, e_r) \\
&\quad + \mathcal{O}_h(\mathbf{v}, \mathbf{c}; \mathbf{u}, \mathbf{b}; \boldsymbol{\xi}_\mathbf{u}, \boldsymbol{\xi}_\mathbf{b}) - \mathcal{O}_h(\mathbf{u}, \mathbf{b}; \mathbf{u}, \mathbf{b}; \boldsymbol{\xi}_\mathbf{u}, \boldsymbol{\xi}_\mathbf{b}) \\
&\quad - \mathcal{O}_h(\mathbf{u}_h, \mathbf{b}_h; \boldsymbol{\eta}_\mathbf{u}, \boldsymbol{\eta}_\mathbf{b}; \boldsymbol{\xi}_\mathbf{u}, \boldsymbol{\xi}_\mathbf{b}).
\end{aligned} \quad (4.20)$$

From the coercivity of $\mathcal{A}_h$ in (3.7) and the continuity of $\mathcal{O}_h$ in Proposition 4.8(i), the left-hand side of Eq. (4.20) can be bounded by

$$\begin{aligned}
\text{l.h.s. of (4.20)} &\geqslant C_C \|(\boldsymbol{\xi}_\mathbf{u}, \boldsymbol{\xi}_\mathbf{b})\|^2_{V_h \times C_h} \\
&\quad - \frac{C_\mathcal{O} \bar\kappa}{\bar{v}^{\frac{3}{2}}} \|(\mathbf{u}, \mathbf{b})\|_{V_h \times C_h} \|(\boldsymbol{\xi}_\mathbf{u}, \boldsymbol{\xi}_\mathbf{b})\|^2_{V_h \times C_h}.
\end{aligned}$$

Next, we estimate $\|(\mathbf{u}, \mathbf{b})\|_{V_h \times C_h}$ using the stability bound in Theorem 2.1 (noting that $\|(\mathbf{u}, \mathbf{b})\|_{V_h \times C_h} \leqslant \|(\mathbf{u}, \mathbf{b})\|_{V \times C}$). We obtain

$$\text{l.h.s. of (4.20)} \geqslant \left(C_C - \frac{c_2 C_\mathcal{O} \bar\kappa \||(\mathbf{f}, \mathbf{g})|\|}{\bar{v}^2} \right) \|(\boldsymbol{\xi}_\mathbf{u}, \boldsymbol{\xi}_\mathbf{b})\|^2_{V_h \times C_h}.$$

In view of assumption (4.19), we then have

$$\text{l.h.s. of (4.20)} \geqslant \frac{1}{2} C_C \|(\boldsymbol{\xi}_\mathbf{u}, \boldsymbol{\xi}_\mathbf{b})\|^2_{V_h \times C_h}.$$

For the right-hand side of (4.20), we note that (since $\xi_\mathbf{u}$ and $\xi_\mathbf{b}$ are in the kernels $\mathbf{J}_h$ and $\mathbf{X}_h$, respectively)

$$\mathcal{B}(\xi_\mathbf{u}, \xi_\mathbf{b}; e_p, e_r) = \mathcal{B}\big(\xi_\mathbf{u}, \xi_\mathbf{b}; \eta_p, \eta_r\big).$$

Then, to bound the right-hand side of (4.20), we use the continuity properties of $\widetilde{\mathcal{A}}_h$, $\mathcal{B}$ and $\mathcal{O}_h$ in (4.3), (4.4) and Proposition 4.8, respectively, as well as the estimate for $\mathcal{R}_A(\xi_\mathbf{u})$ in (4.17). We readily obtain

$$
\begin{aligned}
\text{r.h.s. of } (4.20) \leqslant{} & \|(\xi_\mathbf{u}, \xi_\mathbf{b})\|_{V_h \times C_h} \Big(\mathcal{E}(\mathbf{u}) + C\|(\eta_\mathbf{u}, \eta_\mathbf{b})\|_{V_h \times C_h} \\
& + \|(\eta_p, \eta_r)\|_{Q \times S} + C_d\, \ell(d) \frac{C_{\mathcal{O}}\bar{\kappa}}{\overline{\gamma^2}} \|(\eta_\mathbf{u}, \eta_\mathbf{b})\|_{V_h \times C_h} \|(\mathbf{u}, \mathbf{b})\|_{V \times C} \\
& + \frac{C_{\mathcal{O}}\bar{\kappa}}{\overline{\gamma^2}} \|(\mathbf{u}_h, \mathbf{b}_h)\|_{V_h \times C_h} \|(\eta_\mathbf{u}, \eta_\mathbf{b})\|_{V_h \times C_h} \Big).
\end{aligned}
$$

Next, we employ the stability bounds in Theorems 2.1 and 3.2 for $\|(\mathbf{u}, \mathbf{b})\|_{V \times C}$ and $\|(\mathbf{u}_h, \mathbf{b}_h)\|_{V_h \times C_h}$, respectively, apply the small data assumption (4.19), and combine the lower and upper bounds of (4.20) into the estimate

$$\|(\xi_\mathbf{u}, \xi_\mathbf{b})\|_{V_h \times C_h} \leqslant C_d\, \ell(d) \|(\eta_\mathbf{u}, \eta_\mathbf{b})\|_{V_h \times C_h} + C\Big(\mathcal{E}(\mathbf{u}) + \|(\eta_p, \eta_r)\|_{Q \times S} \Big).$$

From the triangle inequality, we thus obtain the error bound

$$
\begin{aligned}
\|(\mathbf{u} - \mathbf{u}_h, \mathbf{b} - \mathbf{b}_h)\|_{V_h \times C_h} \leqslant{} & C_d\, \ell(d)\, \|(\mathbf{u} - \mathbf{v}, \mathbf{b} - \mathbf{c})\|_{V_h \times C_h} \\
& + C\big(\mathcal{E}(\mathbf{u}) + \|(p - q, r - s)\|_{Q \times S}\big) \quad (4.21)
\end{aligned}
$$

for any $(\mathbf{v}, \mathbf{c}) \in \mathbf{J}_h \times \mathbf{X}_h$, $(q, s) \in Q_h \times S_h$.

Step 2. Next, we replace $(\mathbf{v}, \mathbf{c}) \in \mathbf{J}_h \times \mathbf{X}_h$ in (4.18) by $(\mathbf{v}, \mathbf{c}) \in \mathbf{V}_h \times \mathbf{C}_h$. To that end, let $(\mathbf{v}, \mathbf{c}) \in \mathbf{V}_h \times \mathbf{C}_h$ and we look for $(\mathbf{w}, \mathbf{d}) \in \mathbf{V}_h \times \mathbf{C}_h$ such that

$$\mathcal{B}(\mathbf{w}, \mathbf{d}; q, s) = \mathcal{B}(\mathbf{u} - \mathbf{v}, \mathbf{b} - \mathbf{c}; q, s) \quad \forall\, (q, s) \in Q_h \times S_h.$$

Since the right-hand side is a continuous functional on $Q_h \times S_h$, we conclude from the inf–sup condition of $\mathcal{B}$ in (3.11) that there exists at least one non-trivial solution $(\mathbf{w}, \mathbf{d})$ of this problem satisfying the bound

$$\|(\mathbf{w}, \mathbf{d})\|_{V_h \times C_h} \leqslant C\|(\mathbf{u} - \mathbf{v}, \mathbf{b} - \mathbf{c})\|_{V_h \times C_h}.$$

By construction $(\mathbf{w} + \mathbf{v}, \mathbf{d} + \mathbf{c}) \in \mathbf{J}_h \times \mathbf{X}_h$. Therefore, it can be inserted into (4.21). With the help of the triangle inequality, we readily see that

$$
\begin{aligned}
\|(\mathbf{u} - \mathbf{u}_h, \mathbf{b} - \mathbf{b}_h)\|_{V_h \times C_h} \leqslant{} & \|(\mathbf{u} - \mathbf{v}, \mathbf{b} - \mathbf{c})\|_{V_h \times C_h} \\
& + \|(\mathbf{w} + \mathbf{v} - \mathbf{u}_h, \mathbf{d} + \mathbf{c} - \mathbf{b}_h)\|_{V_h \times C_h} \\
& + \|(\mathbf{w}, \mathbf{d})\|_{V_h \times C_h} \\
\leqslant{} & C_d\, \ell(d) \|(\mathbf{u} - \mathbf{v}, \mathbf{b} - \mathbf{c})\|_{V_h \times C_h} \\
& + C\big(\mathcal{E}(\mathbf{u}) + \|(p - q, r - s)\|_{Q \times S}\big).
\end{aligned}
$$

This completes the proof. □

Next, we present the following result for the multipliers.

Lemma 4.10. *Assume (4.19). Then there holds*

$$
\begin{aligned}
\|(p - p_h, r - r_h)\|_{Q \times S} \leqslant{} & C\Big(\mathcal{E}(\mathbf{u}) + \inf_{(q,s) \in Q_h \times S_h} \|(p - q, r - s)\|_{Q \times S} \\
& + \|(\mathbf{u} - \mathbf{u}_h, \mathbf{b} - \mathbf{b}_h)\|_{V_h \times C_h} \\
& + \sup_{(\mathbf{v}, \mathbf{c}) \in \mathbf{V}_h \times \mathbf{C}_h} \frac{|C(\mathbf{b} - \mathbf{b}_h, \mathbf{v}, \mathbf{b}) - C(\mathbf{b} - \mathbf{b}_h, \mathbf{u}, \mathbf{c})|}{\|(\mathbf{v}, \mathbf{c})\|_{V_h \times C_h}} \Big).
\end{aligned}
$$

Proof. For any $(q, s) \in Q_h \times S_h$, we recall from (4.18) that

$$e_p = \xi_p + \eta_p, \quad e_r = \xi_r + \eta_r.$$

The inf–sup condition for $\mathcal{B}$ in (3.11) and the triangle inequality guarantee that

$$\|(\xi_p, \xi_r)\|_{Q \times S} \leqslant C \sup_{(\mathbf{v}, \mathbf{c}) \in \mathbf{V}_h \times \mathbf{C}_h} \frac{\mathcal{B}(\mathbf{v}, \mathbf{c}; \xi_p, \xi_r)}{\|(\mathbf{v}, \mathbf{c})\|_{V_h \times C_h}} \leqslant C(T_1 + T_2),$$

where

$$
\begin{aligned}
T_1 &= \sup_{(\mathbf{v}, \mathbf{c}) \in \mathbf{V}_h \times \mathbf{C}_h} \frac{\mathcal{B}(\mathbf{v}, \mathbf{c}; \eta_p, \eta_r)}{\|(\mathbf{v}, \mathbf{c})\|_{V_h \times C_h}}, \\
T_2 &= \sup_{(\mathbf{v}, \mathbf{c}) \in \mathbf{V}_h \times \mathbf{C}_h} \frac{\mathcal{B}(\mathbf{v}, \mathbf{c}; e_p, e_r)}{\|(\mathbf{v}, \mathbf{c})\|_{V_h \times C_h}}.
\end{aligned}
$$

Using the continuity of $\mathcal{B}$ in (4.4), T_1 can be easily bounded by

$$T_1 \leqslant C\|(\eta_p, \eta_r)\|_{Q \times S}.$$

For T_2, we make use of the weak formulation and the residual Eq. (4.16) and write out the form $\mathcal{O}_h$ into its individual parts. We obtain

$$
\begin{aligned}
\mathcal{B}(\mathbf{v}, \mathbf{c}; e_p, e_r) ={} & \mathcal{R}_A(\mathbf{v}) - \widetilde{\mathcal{A}}_h(\mathbf{e}_\mathbf{u}, \mathbf{e}_\mathbf{b}; \mathbf{v}, \mathbf{c}) - \mathcal{O}_h(\mathbf{u}_h, \mathbf{b}_h; \mathbf{e}_\mathbf{u}, \mathbf{e}_\mathbf{b}; \mathbf{v}, \mathbf{c}) \\
& - \mathcal{O}_h(\mathbf{u}, \mathbf{b}; \mathbf{u}, \mathbf{b}; \mathbf{v}, \mathbf{c}) + \mathcal{O}_h(\mathbf{u}_h, \mathbf{b}_h; \mathbf{u}, \mathbf{b}; \mathbf{v}, \mathbf{c}) \\
={} & \mathcal{R}_A(\mathbf{v}) - \widetilde{\mathcal{A}}_h(\mathbf{e}_\mathbf{u}, \mathbf{e}_\mathbf{b}; \mathbf{v}, \mathbf{c}) - \mathcal{O}_h(\mathbf{u}_h, \mathbf{b}_h; \mathbf{e}_\mathbf{u}, \mathbf{e}_\mathbf{b}; \mathbf{v}, \mathbf{c}) \\
& - O_h(\mathbf{u}, \mathbf{u}, \mathbf{v}) + O_h(\mathbf{u}_h, \mathbf{u}, \mathbf{v}) - C(\mathbf{e}_\mathbf{b}, \mathbf{v}, \mathbf{b}) \\
& + C(\mathbf{e}_\mathbf{b}, \mathbf{u}, \mathbf{c}).
\end{aligned}
$$

Applying the bound (4.17) and the continuity properties of $\widetilde{\mathcal{A}}_h$, $\mathcal{O}_h$ and O_h in (4.3), Proposition 4.8(i) and Lemma 4.6, respectively, we conclude that

$$
\begin{aligned}
T_2 \leqslant{} & \mathcal{E}(\mathbf{u}) + C\|(\mathbf{e}_\mathbf{u}, \mathbf{e}_\mathbf{b})\|_{V_h \times C_h} + \frac{C_{\mathcal{O}}\bar{\kappa}}{\overline{\gamma^2}} \|(\mathbf{e}_\mathbf{u}, \mathbf{e}_\mathbf{b})\|_{V_h \times C_h} \|(\mathbf{u}_h, \mathbf{b}_h)\|_{V_h \times C_h} \\
& + \frac{C_{\mathcal{O}}\bar{\kappa}}{\overline{\gamma^2}} \|(\mathbf{e}_\mathbf{u}, \mathbf{0})\|_{V_h \times C_h} \|(\mathbf{u}, \mathbf{0})\|_{V_h \times C_h} \\
& + \sup_{(\mathbf{v}, \mathbf{c}) \in \mathbf{V}_h \times \mathbf{C}_h} \frac{|C(\mathbf{e}_\mathbf{b}, \mathbf{v}, \mathbf{b}) - C(\mathbf{e}_\mathbf{b}, \mathbf{u}, \mathbf{c})|}{\|(\mathbf{v}, \mathbf{c})\|_{V_h \times C_h}}.
\end{aligned}
$$

Using the small data assumption (4.19), the assertion follows. □

4.4. Proof of Theorem 4.2

In this subsection, we prove the convergence result stated in Theorem 4.2.

In view of Lemma 4.9, the convergence of $\mathbf{u}_h$ and $\mathbf{b}_h$ is obtained under the smoothness assumption (4.1) by using the standard approximation properties of the finite element spaces $\mathbf{V}_h$, $\mathbf{C}_h$, Q_h and S_h, respectively. This proves the first statement of Theorem 4.2.

Next, we show the convergence of the multipliers in the energy norm $\|\cdot\|_{Q \times S}$. From Lemmas 4.10 and 4.9, it only remains to show that

$$\sup_{(\mathbf{v}, \mathbf{c}) \in \mathbf{V}_h \times \mathbf{C}_h} \frac{|C(\mathbf{b} - \mathbf{b}_h, \mathbf{v}, \mathbf{b}) - C(\mathbf{b} - \mathbf{b}_h, \mathbf{u}, \mathbf{c})|}{\|(\mathbf{v}, \mathbf{c})\|_{V_h \times C_h}} \to 0 \quad \text{as } h \to 0. \quad (4.22)$$

Recalling the Hodge operator $\mathbf{H}$ from (4.9), we write

$$C(\mathbf{b} - \mathbf{b}_h, \mathbf{v}, \mathbf{b}) = C(\mathbf{b} - \mathbf{H}\mathbf{b}_h, \mathbf{v}, \mathbf{b}) + C(\mathbf{H}\mathbf{b}_h - \mathbf{b}_h, \mathbf{v}, \mathbf{b}). \quad (4.23)$$

The first term on the right-hand side of (4.23) tends to zero due to Lemma 4.7(i) and the fact that

$$\|\mathbf{b} - \mathbf{H}\mathbf{b}_h\|_{H(\mathrm{curl};\Omega)} \leqslant \|\mathbf{b} - \mathbf{b}_h\|_{H(\mathrm{curl};\Omega)} + \|\mathbf{b}_h - \mathbf{H}\mathbf{b}_h\|_{H(\mathrm{curl};\Omega)} \to 0$$

as $h \to 0$. Here, we have applied the triangle inequality, the properties of the Hodge operator (4.9) and (4.10), and the stability bound in Theorem 3.2. For the last term of (4.23), we first utilize item (iv) of Lemma 4.7 and then the approximation result (4.10), to get

$$|C(\mathbf{Hb}_h - \mathbf{b}_h, \mathbf{v}, \mathbf{b})| \leqslant Ch^{-\frac{1}{2}}\kappa\|\mathbf{Hb}_h - \mathbf{b}_h\|_{L^2(\Omega)}\|\mathbf{v}\|_{1,h}\|\mathbf{b}\|_{H(\mathrm{curl};\Omega)}$$

$$\leqslant Ch^{\tau-\frac{1}{2}}\kappa\|\nabla \times \mathbf{b}_h\|_{L^2(\Omega)}\|\mathbf{v}\|_{1,h}\|\mathbf{b}\|_{H(\mathrm{curl};\Omega)}$$

$$\leqslant Ch^{\tau-\frac{1}{2}}\frac{\kappa}{\bar{\nu}^{\frac{3}{2}}}\|(\mathbf{0},\mathbf{b}_h)\|_{V_h \times C_h}\|(\mathbf{v},\mathbf{0})\|_{V_h \times C_h}\|(\mathbf{0},\mathbf{b})\|_{V \times C}$$

$$\leqslant Ch^{\tau-\frac{1}{2}}\|(\mathbf{v},\mathbf{0})\|_{V_h \times C_h}\frac{\||(\mathbf{f},\mathbf{g})\||}{\bar{\nu}^{\frac{1}{2}}}.$$

In the last step, we have applied the stability bounds in Theorems 2.1 and 3.2, as well as the small data assumption (4.19). Since $\bar{\nu}^{-\frac{1}{2}}\||(\mathbf{f},\mathbf{g})\|| \leqslant \bar{\kappa}\bar{\nu}^{-2}\||(\mathbf{f},\mathbf{g})\||$ and $\tau > \frac{1}{2}$, we obtain

$$\sup_{(\mathbf{v},\mathbf{c})\in V_h \times C_h}\frac{|C(\mathbf{b}-\mathbf{b}_h,\mathbf{v},\mathbf{b})|}{\|(\mathbf{v},\mathbf{c})\|_{V_h \times C_h}} \to 0 \quad \text{as } h \to 0.$$

A similar argument shows that

$$\sup_{(\mathbf{v},\mathbf{c})\in V_h \times C_h}\frac{|C(\mathbf{b}-\mathbf{b}_h,\mathbf{u},\mathbf{c})|}{\|(\mathbf{v},\mathbf{c})\|_{V_h \times C_h}} \to 0 \quad \text{as } h \to 0.$$

Therefore (4.22) holds true, and the convergence of the multipliers is obtained.

4.5. Proof of Theorem 4.3

In this subsection we prove the a priori error estimates in Theorem 4.3. As before, we consider the cases $d = 2$ and $d = 3$ simultaneously.

Based on Lemma 4.9, we choose $\mathbf{v}$ as the BDM projection of $\mathbf{u}$, $\mathbf{c}$ the Nédélec projection of $\mathbf{b}$, q and s the L^2-projections of p and r, respectively. We then apply the approximation properties of these projections in [7, Proposition III.3.6], [40, Theorem 5.41] and [8], and the estimates for the errors in the velocity and magnetic fields are readily obtained.

To prove the error estimate for the multipliers, we first apply Proposition 4.8 (ii) to bound the supremum in the estimate of Lemma 4.10:

$$\sup_{(\mathbf{v},\mathbf{c})\in V_h \times C_h}\frac{|C(\mathbf{b}-\mathbf{b}_h,\mathbf{v},\mathbf{b}) - C(\mathbf{b}-\mathbf{b}_h,\mathbf{u},\mathbf{c})|}{\|(\mathbf{v},\mathbf{c})\|_{V_h \times C_h}}$$

$$\leqslant C_d\,\ell(d)\frac{C_{\mathcal{O}}\bar{\kappa}}{\bar{\nu}^{\frac{3}{2}}}\|(\mathbf{0},\mathbf{b}-\mathbf{b}_h)\|_{V_h \times C_h}\|(\mathbf{u},\mathbf{b})\|_{V \times C}.$$

Utilizing the stability bound in Theorem 2.1, we obtain

$$\|(p-p_h, r-r_h)\|_{Q \times S} \leqslant C\left(\mathcal{E}(\mathbf{u}) + \inf_{(q,s)\in Q_h \times S_h}\|(p-q, r-s)\|_{Q \times S}\right)$$

$$+ C_d\ell(d)\|(\mathbf{u}-\mathbf{u}_h, \mathbf{b}-\mathbf{b}_h)\|_{V_h \times C_h}$$

$$\leqslant C_d\ell(d)^2 \inf_{(\mathbf{v},\mathbf{c})\in V_h \times C_h}\|(\mathbf{u}-\mathbf{v}, \mathbf{b}-\mathbf{c})\|_{V_h \times C_h}$$

$$+ C_d\ell(d)\left(\mathcal{E}(\mathbf{u}) + \inf_{(q,s)\in Q_h \times S_h}\|(p-q, r-s)\|_{Q \times S}\right).$$

Again, we choose $\mathbf{v}$ as the BDM projection of $\mathbf{u}$, $\mathbf{c}$ the Nédélec projection of $\mathbf{b}$, q and s the L^2-projections of p and r, respectively. As before, the approximation properties of these projections finish the proof.

5. Numerical results

In this section we present a series of numerical experiments. Our computations have been carried out using MATLAB, with direct linear solvers. The primary purpose of our experiments is to confirm optimal convergence rates of our method. We start by considering one problem with a smooth solution and a second one with a singular solution. Then, we consider the numerical approximations of two- and three-dimensional Hartmann channel flow and driven cavity flow problems. Finally, we present results for another benchmark problem: MHD flow over a step in two dimensions.

Throughout this section, the lowest order BDM and Nédélec elements are employed and the interior penalty stabilization parameter is $a_0 = 10$. The Picard iteration described in Section 4.5 is used to solve the non-linear systems. For all the examples, we solve a Stokes problem and the Maxwell equations, decoupled, to obtain an initial guess. The tolerance for the Picard iterations is chosen as 1e−5.

We test our method on problems with mixed Dirichlet and Neumann boundary conditions in the hydrodynamic variables, even though the analysis has been carried out solely for the Dirichlet case. Throughout this section, Γ_N denotes the Neumann boundary, and Γ_D the Dirichlet boundary. On Neumann boundaries, we specify the value of $(p\underline{\mathbf{I}} - \nu\nabla\mathbf{u})\mathbf{n}$, where $\underline{\mathbf{I}}$ is the identity matrix.

5.1. Example 1: two-dimensional problem with a smooth solution

First, we verify the theoretical results stated in Theorems 4.2 and 4.3 for a problem with a smooth analytical solution.

We consider the following two-dimensional problem. We set $\Omega = (-1,1)^2$ with $\Gamma_N = \{(1,y): y \in (-1,1)\}$, $\Gamma_D = \partial\Omega\backslash\Gamma_N$, $\nu = \kappa = 1$, $\nu_m = 1e4$, and choose the source terms $\mathbf{f}, \mathbf{g}$ and the boundary conditions so that the analytical solution is of the form

$$\mathbf{u}(x,y) = (y^2, x^2), \quad p(x,y) = x,$$
$$\mathbf{b}(x,y) = (1-y^2, 1-x^2), \quad r(x,y) = (1-x^2)(1-y^2).$$

We construct this example with $r \neq 0$ to show the convergence rate in r_h; later examples will feature a divergence-free $\mathbf{g}$ and a vanishing r; cf. Proposition 3.1.

In Tables 5.1–5.3, we investigate the asymptotic rates of convergence of the errors in the approximations of the hydrodynamic and magnetic variables; here, l denotes the experimental rate of convergence. We observe that $\|\mathbf{u}-\mathbf{u}_h\|_{1,h}$, $\|p-p_h\|_{L^2(\Omega)}$, $\|\mathbf{b}-\mathbf{b}_h\|_{H(\mathrm{curl};\Omega)}$ and $\|\nabla(r-r_h)\|_{L^2(\Omega)}$ converge to zero as the mesh is refined, in accordance with Theorem 4.2. The rate of convergence is $\mathcal{O}(h)$. Notice that we obtain the optimal rate in this numerical experiment, even though Theorem 4.3 predicts a sub-optimal rate with a loss of $\mathcal{O}(h^\varepsilon)$. Additionally, $\|\mathbf{u}-\mathbf{u}_h\|_{L^2(\Omega)}$ and $\|r-r_h\|_{L^2(\Omega)}$ converge at rate $\mathcal{O}(h^2)$ as h tends to zero, which is also optimal.

Table 5.1
Example 1. Convergence of $\|\mathbf{u}-\mathbf{u}_h\|_{L^2(\Omega)}$, $\|\mathbf{u}-\mathbf{u}_h\|_{1,h}$, and $\|p-p_h\|_{L^2(\Omega)}$.

Dofs in $\mathbf{u}_h$/ p_h	$\|\mathbf{u}-\mathbf{u}_h\|_{L^2(\Omega)}$	l	$\|\mathbf{u}-\mathbf{u}_h\|_{1,h}$	l	$\|p-p_h\|_{L^2(\Omega)}$	l
112/32	3.893e−2	–	8.297e−1	–	1.297	–
416/128	1.016e−2	1.94	4.105e−1	1.01	3.734e−1	1.78
1600/512	2.707e−3	1.91	2.045e−1	1.01	1.293e−1	1.53
6272/2048	7.087e−4	1.93	1.021e−1	1.00	5.475e−2	1.24
24,832/ 8192	1.813e−4	1.97	5.104e−2	1.00	2.597e−2	1.08
98,816/ 32,768	4.578e−5	1.99	2.552e−2	1.00	1.281e−2	1.02

Table 5.2
Example 1. Convergence of $\|\mathbf{b}-\mathbf{b}_h\|_{L^2(\Omega)}$ and $\|\mathbf{b}-\mathbf{b}_h\|_{H(\mathrm{curl};\Omega)}$.

Dofs in $\mathbf{b}_h$/r_h	$\|\mathbf{b}-\mathbf{b}_h\|_{L^2(\Omega)}$	l	$\|\mathbf{b}-\mathbf{b}_h\|_{H(\mathrm{curl};\Omega)}$	l
56/25	4.720e−1	–	9.431e−1	–
208/81	2.358e−1	1.00	4.714e−1	1.00
800/289	1.179e−1	1.00	2.357e−1	1.00
3136/1089	5.893e−2	1.00	1.179e−1	1.00
12,416/4225	2.946e−2	1.00	5.893e−2	1.00
49,408/16,641	1.473e−2	1.00	2.946e−2	1.00

Table 5.3
Example 1. Convergence of $\|r - r_h\|_{L^2(\Omega)}$ and $\|\nabla(r - r_h)\|_{L^2(\Omega)}$.

Dofs in $\mathbf{b}_h/r_h$	$\|r - r_h\|_{L^2(\Omega)}$	l	$\|\nabla(r - r_h)\|_{L^2(\Omega)}$	l
56/25	1.673e−1	–	9.391e−1	–
208/81	4.433e−2	1.92	4.824e−1	0.96
800/289	1.125e−2	1.98	2.429e−1	0.99
3136/1089	2.822e−3	1.99	1.216e−1	1.00
12,416/4225	7.062e−4	2.00	6.085e−2	1.00
49,408/16,641	1.766e−4	2.00	3.043e−2	1.00
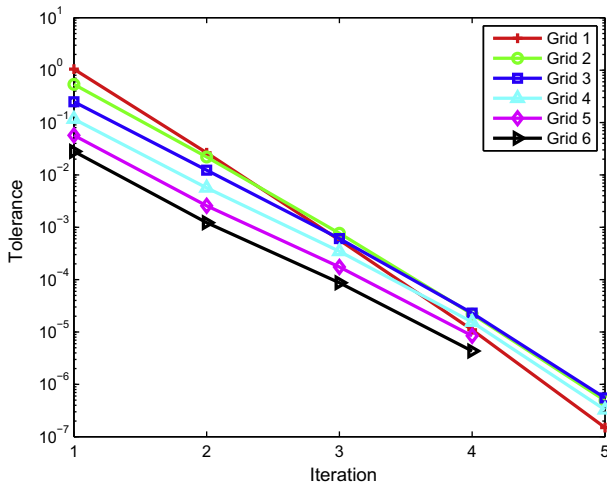
Fig. 5.1. Example 1. Convergence history of the Picard iteration for the grid sequence defined in Tables 5.1–5.3.

In Fig. 5.1 we show the convergence history of the Picard iterations for the grid sequence considered in this example. The plot depicts the number of iterations against the differences between consecutive iterates corresponding to the approximated vector coefficients, measured in a normalized discrete 2-norm and labeled as 'Tolerance' in the plot. As expected, convergence is linear and the iteration count is fairly insensitive to the size of the grid. A very similar behavior has been observed in all of our other experiments, in 2D as well as in 3D.

5.2. Example 2: two-dimensional problem with a singular solution

In order to verify the capability of the proposed method to capture singularities in two dimensions, we consider a problem in the L-shaped domain $\Omega = (-1,1)^2\backslash([0,1) \times (-1,0])$ with $\Gamma_N = \{(1,y): y \in (0,1)\}$, $\Gamma_D = \partial\Omega \setminus \Gamma_N$, and set $\nu = \kappa = 1$, ν_m1e4. We choose the forcing terms and the boundary conditions such that the analytic solution is given by the strongest corner singularities for the underlying elliptic operators. In polar coordinates (ρ, ϕ), the hydrodynamic solution components $\mathbf{u}$ and p are then given by

$$\mathbf{u}(\rho, \phi) = \begin{bmatrix} \rho^\lambda((1 + \lambda)\sin(\phi)\psi(\phi) + \cos(\phi)\psi'(\phi)) \\ \rho^\lambda(-(1 + \lambda)\cos(\phi)\psi(\phi) + \sin(\phi)\psi'(\phi)) \end{bmatrix},$$

$$p(\rho, \phi) = -\rho^{\lambda-1}\left((1 + \lambda)^2\psi'(\phi) + \psi'''(\phi)\right)/(1 - \lambda),$$

where

$$\psi(\phi) = \sin((1 + \lambda)\phi)\cos(\lambda\omega)/(1 + \lambda) - \cos((1 + \lambda)\phi)$$
$$- \sin((1 - \lambda)\phi)\cos(\lambda\omega)/(1 - \lambda) + \cos((1 - \lambda)\phi),$$

$\omega = \frac{3}{2}\pi$ and $\lambda \approx 0.54448373678246$. The magnetic pair $(\mathbf{b}, r)$ is given by

$$\mathbf{b}(\rho, \phi) = \nabla(\rho^{2/3}\sin(2/3\phi)), \quad r(\rho, \phi) \equiv 0.$$

For this example, we have that $(\mathbf{u}, p) \in H^{1 + \lambda}(\Omega)^2 \times H^\lambda(\Omega)$ and $\mathbf{b} \in H^{2/3}(\Omega)^2$. Note that straightforwardly applied nodal elements cannot correctly resolve the magnetic field. In Tables 5.4 and 5.5, we investigate the asymptotic rates of convergence of the errors in the approximations of the hydrodynamic and magnetic variables. Again, we observe that the discrete solution converges to the exact one as the mesh size h approaches zero, in accordance with Theorem 4.2. The results show full agreement with the optimal rates for $\|\mathbf{u} - \mathbf{u}_h\|_{1,h}$ and $\|\mathbf{b} - \mathbf{b}_h\|_{H(\text{curl};\Omega)}$. For the pressure, we also see that the rate for $\|p - p_h\|_{L^2(\Omega)}$ is approaching the optimal rate, albeit more slowly. Additionally, we observe the L^2-norm of r is zero because $\mathbf{g}$ is divergence-free, in accordance with Proposition 3.1.

In Figs. 5.2 and 5.3, we show the solution computed on the finest mesh with 24,576 elements; the total number of degrees of freedom employed in the finite element space $\mathbf{V}_h \times \mathbf{C}_h \times Q_h \times S_h$ is 148,481. The results show that our solution captures the strongest corner singularities and are comparable to the results in [36].

5.3. Hartmann channel flow

Next, we consider Hartmann channel flow problems in two and three dimensions; cf. [26]. In these examples, we denote by Ha the Hartmann number, which is defined as $\text{Ha} = \sqrt{\frac{\kappa}{\nu\nu_m}}$.

5.3.1. Example 3: two-dimensional Hartmann flow

Consider the two-dimensional Hartmann flow problem, which involves a steady unidirectional flow in the channel $\Omega = (0,10) \times (-1,1)$ under the influence of the constant transverse magnetic field $\mathbf{b}_D = (0,1)$. The MHD solution then takes the form:

$$\mathbf{u}(x,y) = (u(y), 0), \quad p(x,y) = -Gx + p_0(y),$$
$$\mathbf{b}(x,y) = (b(y), 1), \quad r(x,y) \equiv 0. \tag{5.1}$$

We impose the following boundary conditions:

$$\mathbf{u} = \mathbf{0} \qquad \text{on } y = \pm 1,$$
$$(p\mathbf{I} - \nu\nabla\mathbf{u})\mathbf{n} = p_N\mathbf{n} \quad \text{on } x = 0 \text{ and } x = 10,$$
$$\mathbf{n} \times \mathbf{b} = \mathbf{n} \times \mathbf{b}_D \quad \text{on } \partial\Omega,$$
$$r = 0 \qquad \text{on } \partial\Omega,$$

where

$$p_N(x,y) = p(x,y) = -Gx - \frac{G^2}{2\kappa}\left(\frac{\sinh(y\text{Ha})}{\sinh(\text{Ha})} - y\right)^2.$$

The exact solution is given by (5.1) with

$$u(y) = \frac{G}{\nu\text{Ha}\tanh(\text{Ha})}\left(1 - \frac{\cosh(y\text{Ha})}{\cosh(\text{Ha})}\right),$$

$$b(y) = \frac{G}{\kappa}\left(\frac{\sinh(y\text{Ha})}{\sinh(\text{Ha})} - y\right),$$

$$p_0(y) = -\frac{G^2}{2\kappa}\left(\frac{\sinh(y\text{Ha})}{\sinh(\text{Ha})} - y\right)^2.$$

Table 5.4
Example 2. Convergence of $\|\mathbf{u} - \mathbf{u}_h\|_{L^2(\Omega)}$, $\|\mathbf{u} - \mathbf{u}_h\|_{1,h}$, and $\|p - p_h\|_{L^2(\Omega)}$.

Dofs in $\mathbf{u}_h/p_h$	$\|\mathbf{u} - \mathbf{u}_h\|_{L^2(\Omega)}$	l	$\|\mathbf{u} - \mathbf{u}_h\|_{1,h}$	l	$\|p - p_h\|_{L^2(\Omega)}$	l
88/24	2.159e−1	–	2.468	–	15.91	–
320/96	1.781e−1	0.28	1.880	0.39	9.328	0.77
1216/384	1.204e−1	0.56	1.368	0.46	5.387	0.79
4736/1536	6.816e−1	0.82	0.9588	0.51	3.301	0.71
18,688/6144	3.490e−2	0.97	0.6627	0.53	2.124	0.64
74,240/24,576	1.705e−2	1.03	0.4559	0.54	1.408	0.59

Table 5.5
Example 2. Convergence of $\|\mathbf{b}-\mathbf{b}_h\|_{L^2(\Omega)}$, $\|\mathbf{b}-\mathbf{b}_h\|_{H(\mathrm{curl};\Omega)}$, and $\|r_h\|_{L^2(\Omega)}$.

Dofs in $\mathbf{b}_h/r_h$	$\|\mathbf{b}-\mathbf{b}_h\|_{L^2(\Omega)}$	l	$\|\mathbf{b}-\mathbf{b}_h\|_{H(\mathrm{curl};\Omega)}$	l	$\|r_h\|_{L^2(\Omega)}$
44/21	2.796e−1	–	2.796	–	2.162e−12
160/65	1.814e−1	0.62	1.814e−1	0.62	6.188e−12
608/225	1.169e−1	0.63	1.169e−1	0.63	2.289e−11
2368/833	7.473e−2	0.65	7.473e−2	0.65	4.260e−11
9344/3201	4.754e−2	0.65	4.754e−2	0.65	1.406e−10
37,120/12,545	3.013e−2	0.66	3.013e−2	0.66	3.018e−10

Table 5.6
Example 3. Convergence of $\|\mathbf{u}-\mathbf{u}_h\|_{L^2(\Omega)}$, $\|\mathbf{u}-\mathbf{u}_h\|_{1,h}$, and $\|p-p_h\|_{L^2(\Omega)}$.

Dofs in $\mathbf{u}_h/p_h$	$\|\mathbf{u}-\mathbf{u}_h\|_{L^2(\Omega)}$	l	$\|\mathbf{u}-\mathbf{u}_h\|_{1,h}$	l	$\|p-p_h\|_{L^2(\Omega)}$	l
416/128	2.028e−1	–	3.215	–	13.97	–
1600/512	5.169e−2	1.97	1.611	1.00	6.986	1.00
6272/2048	1.306e−2	1.99	0.8061	1.00	3.493	1.00
24,832/8192	3.282e−3	1.99	0.4033	1.00	1.747	1.00
98,816/32,768	8.227e−4	2.00	0.2017	1.00	0.8734	1.00

We note that $p_0(y)$ and $-\frac{\kappa b(y)^2}{2}$ are the same up to an additive constant.

In Tables 5.6, 5.7 and Figs. 5.4, 5.5, we set $v = \kappa = 1$, $v_m = 1\mathrm{e}4$, and $G = 10$. We observe that $r_h \equiv 0$, as predicted in Proposition 3.1, and $\|\mathbf{u}-\mathbf{u}_h\|_{1,h}$, $\|p-p_h\|_{L^2(\Omega)}$ and $\|\mathbf{b}-\mathbf{b}_h\|_{H(\mathrm{curl};\Omega)}$ converge to zero at the optimal rate $\mathcal{O}(h)$ as the mesh is refined. Moreover, we note that the L^2-norms of the errors in the approximations of $\mathbf{u}$, $\mathbf{b}$ and p tend to zero optimally as well.

In Figs. 5.4, 5.5 we show the solution computed on the mesh with 32,768 elements; the total number of degrees of freedom employed in the finite element space $\mathbf{V}_h \times \mathbf{C}_h \times Q_h \times S_h$ is 197,633. In order to show the directions of vectors, in Fig. 5.5(b) and later figures, $\mathbf{b}$ is normalized such that the largest magnitude of each com-

ponent is 1 in the computational domain. The computed and analytical solutions of the first components in the velocity and magnetic fields are virtually indistinguishable; see Fig. 5.4.

5.3.2. Example 4: three-dimensional Hartmann flow

In this example, we consider the three-dimensional unidirectional flow in the rectangular duct given by $\Omega = (0,L) \times (-y_0,y_0) \times (-z_0,z_0)$ with $y_0,z_0 \ll L$ under the influence of the constant transverse magnetic field $\mathbf{b}_D = (0,1,0)$. We take $\mathbf{f} = \mathbf{g} = 0$ and consider solutions of the form

$$\mathbf{u}(x,y,z) = (u(y,z),0,0), \quad p(x,y,z) = -Gx + p_0(y,z),$$
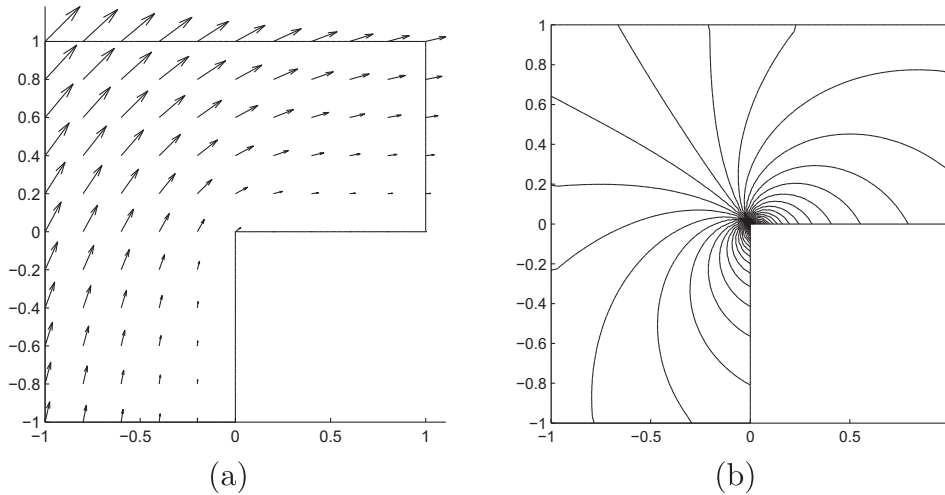$$\mathbf{b}(x,y,z) = (b(y,z),1,0), \quad r(x,y,z) \equiv 0.$$

Fig. 5.2. Example 2. Numerical approximations of (a) velocity; (b) pressure contours.
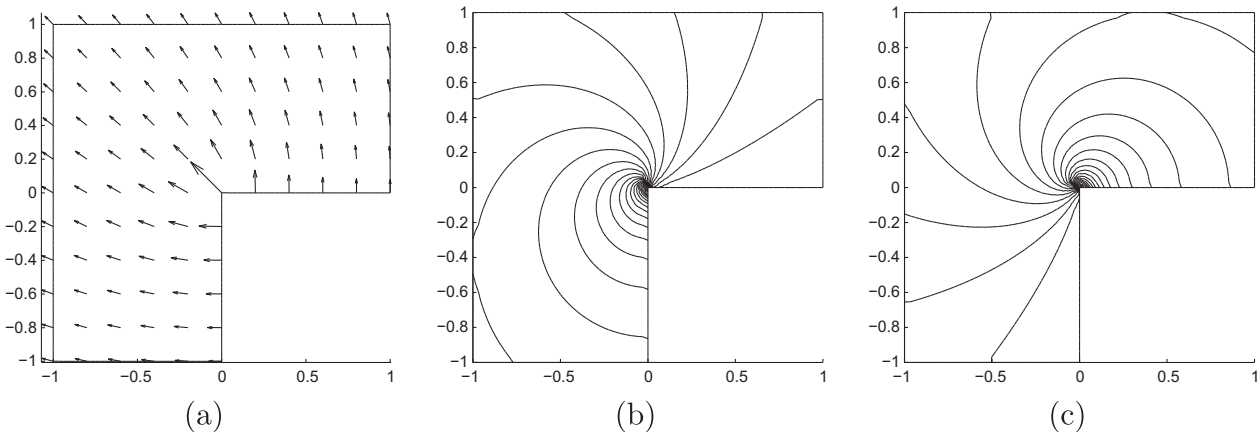

Fig. 5.3. Example 2. Numerical approximations of (a) magnetic field; (b) contours of the first component of the magnetic field and (c) contours of the second component of the magnetic field.

Table 5.7
Example 3. Convergence of $\|\mathbf{b} - \mathbf{b}_h\|_{L^2(\Omega)}$, $\|\mathbf{b} - \mathbf{b}_h\|_{H(\text{curl};\Omega)}$, and $\|r_h\|_{L^2(\Omega)}$.

Dofs in $\mathbf{b}_h/r_h$	$\|\mathbf{b} - \mathbf{b}_h\|_{L^2(\Omega)}$	l	$\|\mathbf{b} - \mathbf{b}_h\|_{H(\text{curl};\Omega)}$	l	$\|r_h\|_{L^2(\Omega)}$
208/81	1.679e−4	–	2.259e−4	–	3.868e−12
800/289	8.605e−5	0.96	1.148e−4	0.98	1.746e−11
3136/1089	4.328e−5	0.99	5.761e−4	0.99	3.627e−11
12,416/4225	2.167e−5	1.00	2.883e−5	1.00	9.424e−11
49,408/16,641	1.084e−5	1.00	1.442e−5	1.00	2.401e−10

Fig. 5.5. Example 3. Numerical approximations of (a) velocity and (b) normalized magnetic field.

We enforce the boundary conditions

$$\mathbf{u} = \mathbf{0} \qquad\qquad \text{for } y = \pm y_0 \text{ and } z = \pm z_0,$$
$$(p\underline{\mathbf{I}} - \nu\nabla\mathbf{u})\mathbf{n} = p_N\mathbf{n} \quad \text{for } x = 0 \text{ and } x = L,$$
$$\mathbf{n} \times \mathbf{b} = \mathbf{n} \times \mathbf{b}_D \quad \text{on } \partial\Omega,$$
$$r = 0 \qquad\qquad \text{on } \partial\Omega$$

with $p_N(x,y,z) = -Gx - \frac{\kappa b(y,z)^2}{2} + 10$. The function $b(y,z)$ is given by the Fourier series

$$b(y,z) = \sum_{n=0}^{\infty} b_n(y) \cos(\lambda_n z),$$

where

$$\lambda_n = \frac{(2n+1)\pi}{2z_0},$$

$$b_n(y) = \frac{\nu}{\kappa}\left(A_n \frac{\lambda_n^2 - p_1^2}{p_1}\sinh(p_1 y) + B_n \frac{\lambda_n^2 - p_2^2}{p_2}\sinh(p_2 y)\right),$$
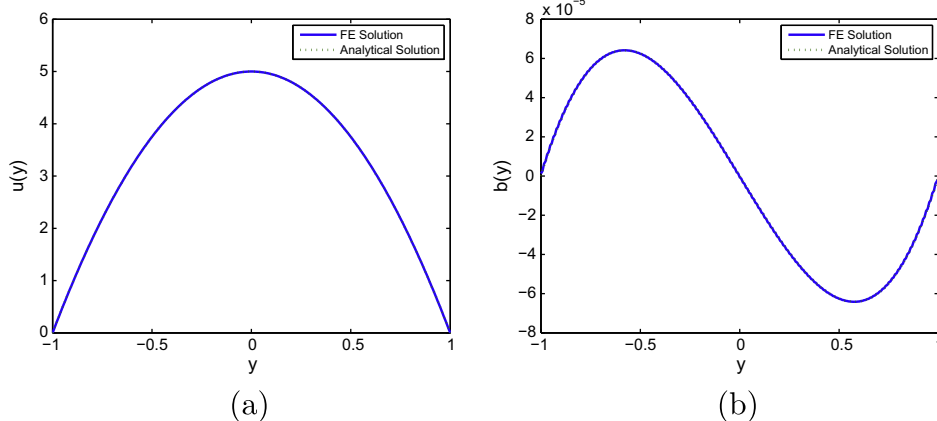
$$p_{1,2}^2 = \lambda_n^2 + \text{Ha}^2/2 \pm \text{Ha}\sqrt{\lambda_n^2 + \text{Ha}^2/4},$$

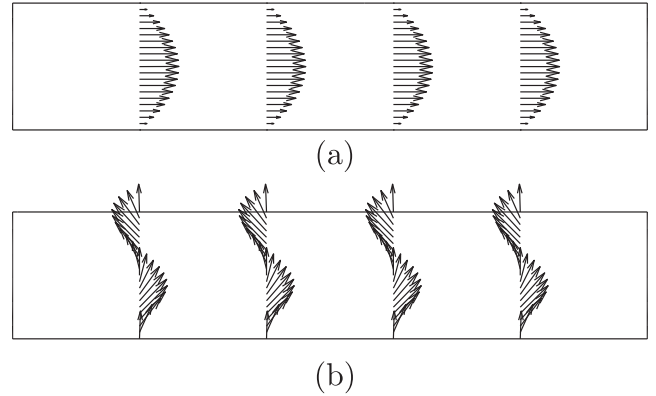$$A_n = \frac{-p_1(\lambda_n^2 - p_2^2)}{\Delta_n} u_n(y_0)\sinh(p_2 y_0),$$

$$B_n = \frac{p_2(\lambda_n^2 - p_1^2)}{\Delta_n} u_n(y_0)\sinh(p_1 y_0),$$

$$\Delta_n = p_2(\lambda_n^2 - p_1^2)\sinh(p_1 y_0)\cosh(p_2 y_0) - p_1(\lambda_n^2 - p_2^2)\sinh(p_2 y_0)$$
$$\times \cosh(p_1 y_0),$$

$$u_n(y_0) = \frac{-2G}{\nu\lambda_n^3 z_0}\sin(\lambda_n z_0).$$

The functions $u(y,z)$ and $p_0(y,z)$ can be also expressed by Fourier series; for details, see [24]. In fact, $p_0(y,z)$ and $-\frac{\kappa b(y,z)^2}{2}$ are identical up to an additive constant. Note also that $p(x,y,z) = p_N(x,y,z)$.

In our tests, we set $L = 10$, $y_0 = 2$, $z_0 = 1$, $\nu = \kappa = 1$, $\nu_m = 1e4$ and $G = 0.5$. In Tables 5.8 and 5.9, we investigate the asymptotic rates of convergence of the errors in the approximations of the hydrodynamic and magnetic variables. Again, we observe that the finite element solution converges to the exact solution as the mesh size h approaches zero, in accordance with Theorem 4.2. We observe the results show good agreement with the optimal rates for $\|\mathbf{u} - \mathbf{u}_h\|_{1,h}$ and $\|\mathbf{b} - \mathbf{b}_h\|_{H(\text{curl};\Omega)}$. For the pressure, we also see that the rate for $\|p - p_h\|_{L^2(\Omega)}$ is approaching the optimal rate, although more slowly. Additionally, we observe the L^2-norm of r is zero because $\mathbf{g}$ is divergence-free, in accordance with Proposition 3.1.

In Figs. 5.6 and 5.7 we show the solution computed on a uniform tetrahedral mesh of 24,576 elements; this results in a total of 212,577 degrees of freedom in the finite element space $\mathbf{V}_h \times \mathbf{C}_h \times Q_h \times S_h$. We observe that the computed and analytical solutions are in good agreement on this relatively coarse mesh; see Fig. 5.6.

5.4. Driven cavity flow

Let us consider a classic test problem used in fluid dynamics, known as driven cavity flow. It is a model of the flow in a cavity with the lid moving in one direction; cf. [23, Chapter 5.1.3] and [43].

Fig. 5.4. Example 3. Slices along $x = 5$, $-1 \leqslant y \leqslant 1$: (a) velocity component $u(y)$ and (b) magnetic component $b(y)$.

Table 5.8
Example 4. Convergence of $\|\mathbf{u} - \mathbf{u}_h\|_{L^2(\Omega)}$, $\|\mathbf{u} - \mathbf{u}_h\|_{1,h}$, and $\|p - p_h\|_{L^2(\Omega)}$.

Dofs in $\mathbf{u}_h$/ p_h	$\|\mathbf{u} - \mathbf{u}_h\|_{L^2(\Omega)}$	l	$\|\mathbf{u} - \mathbf{u}_h\|_{1,h}$	l	$\|p - p_h\|_{L^2(\Omega)}$	l
360/48	3.959e−1	–	1.829	–	30.89	–
2592/384	1.320e−1	1.58	0.9561	0.94	8.194	1.91
19,584/ 3072	3.609e−2	1.87	0.4903	0.96	2.837	1.53
152,064/ 24,576	9.590e−3	1.91	0.2484	0.98	1.091	1.38

Table 5.9
Example 4. Convergence of $\|\mathbf{b} - \mathbf{b}_h\|_{L^2(\Omega)}$, $\|\mathbf{b} - \mathbf{b}_h\|_{H(\text{curl};\Omega)}$, and $\|r_h\|_{L^2(\Omega)}$.

Dofs in $\mathbf{b}_h$/r_h	$\|\mathbf{b} - \mathbf{b}_h\|_{L^2(\Omega)}$	l	$\|\mathbf{b} - \mathbf{b}_h\|_{H(\text{curl};\Omega)}$	l	$\|r_h\|_{L^2(\Omega)}$
98/27	1.850e−5	–	3.219e−5	–	9.855e−12
604/125	1.565e−5	0.24	2.579e−5	0.32	1.013e−10
4184/729	8.592e−6	0.86	1.464e−5	0.82	4.098e−10
31,024/4913	4.411e−6	0.96	7.543e−6	0.96	1.795e−9

5.4.1. Example 5: two-dimensional driven cavity flow

In this example, we consider the two-dimensional domain $\Omega = (-1,1) \times (-1,1)$ with $\Gamma_D = \partial\Omega$, and set the source terms to be zero. The boundary conditions are prescribed as follows:

$$\mathbf{u} = \mathbf{0} \qquad \text{on } x = \pm 1 \quad \text{and } y = -1,$$
$$\mathbf{u} = (1,0) \qquad \text{on } y = 1,$$
$$\mathbf{n} \times \mathbf{b} = \mathbf{n} \times \mathbf{b}_D \quad \text{on } \partial\Omega,$$
$$r = 0 \qquad \text{on } \partial\Omega,$$

where $\mathbf{b}_D = (1,0)$.

We set $\nu = 1e-2$, $\nu_m = 1e5$, $\kappa = 1e5$, which simulate liquid metal type flows. Figs. 5.8 and 5.9 show the solution computed on a mesh with 8192 elements and 49,665 degrees of freedom. Fig. 5.8(a) shows that the circulation created by the moving lid; Fig. 5.8(b) shows the magnetic field changes direction due to the coupling effect. Fig. 5.9(a) demonstrates the boundary layer formation in terms of the first component of the velocity. Streamlines for the velocity field are displayed in Fig. 5.9(b). The computed solution agrees with the solution in the literature [43].

5.4.2. Example 6: three-dimensional driven cavity flow

The problem we consider is the three-dimensional driven cavity flow in the domain $\Omega = (-1,1) \times (-1,1) \times (-1,1)$ with $\Gamma_D = \partial\Omega$. The source terms are set to be zero. The boundary conditions are prescribed as follows:
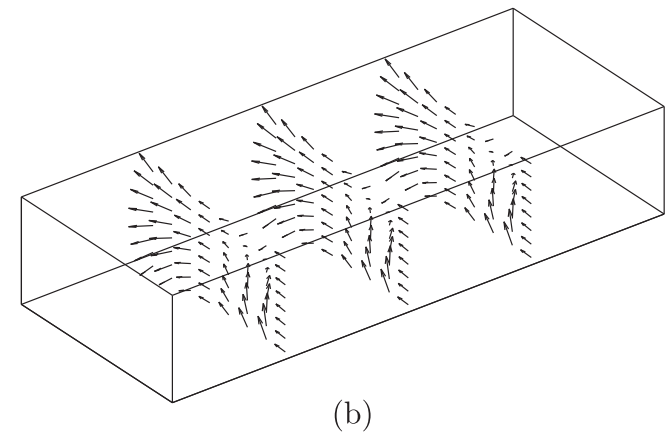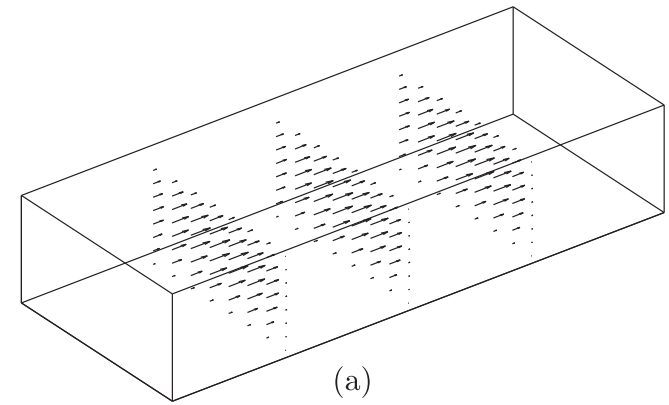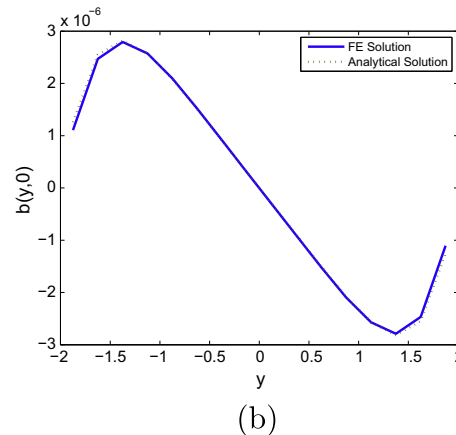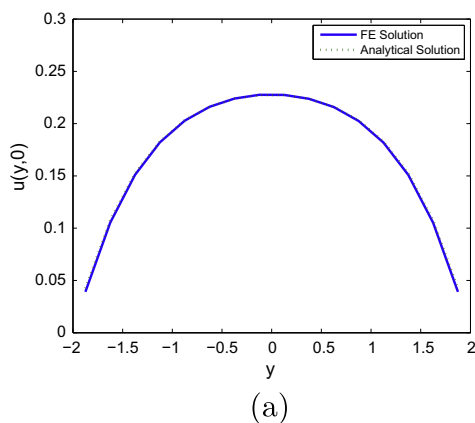

Fig. 5.7. Example 4. Numerical approximations of (a) velocity and (b) normalized magnetic field.

$$\mathbf{u} = \mathbf{0} \qquad \text{on } x = \pm 1, \ y = \pm 1 \quad \text{and } z = -1,$$
$$\mathbf{u} = (1,0,0) \qquad \text{on } z = 1,$$
$$\mathbf{n} \times \mathbf{b} = \mathbf{n} \times \mathbf{b}_D \quad \text{on } \partial\Omega,$$
$$r = 0 \qquad \text{on } \partial\Omega,$$

where $\mathbf{b}_D = (1,0,0)$.

We set $\nu = 1e-2$, $\nu_m = 1e5$, $\kappa = 1e5$ and obtain Fig. 5.10 on a uniform tetrahedral mesh comprising 24,576 elements; this results in a total of 212,577 degrees of freedom. The flow vectors on slices demonstrate a similar behavior to the two-dimensional scenario in Section 5.4.1; see Fig. 5.8.

Fig. 5.6. Example 4. Slices along $x = 5$, $-2 \leqslant y \leqslant 2$, and $z = 0$: (a) velocity component $u(y,0)$ and (b) magnetic component $b(y,0)$.
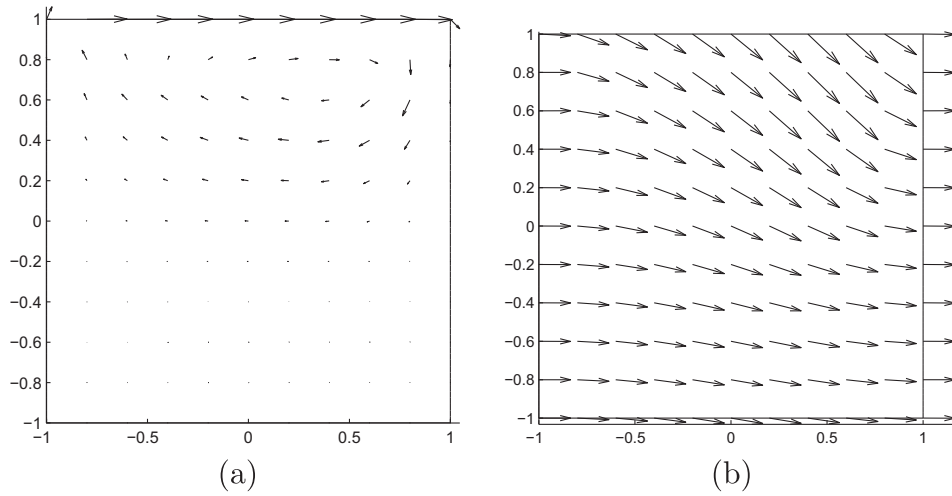
Fig. 5.8. Example 5. Numerical approximations of (a) velocity and (b) normalized magnetic field.
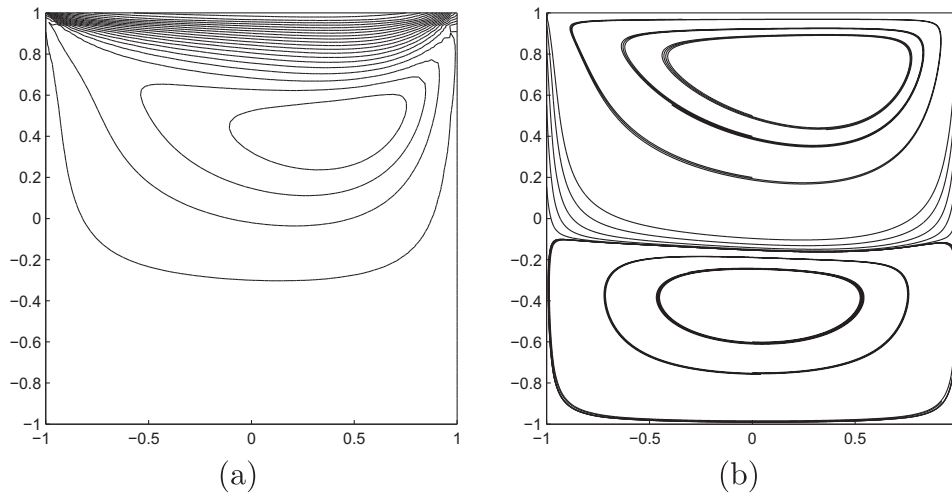

Fig. 5.9. Example 5. Numerical approximations of (a) contours of first velocity components; (b) streamlines of velocity.
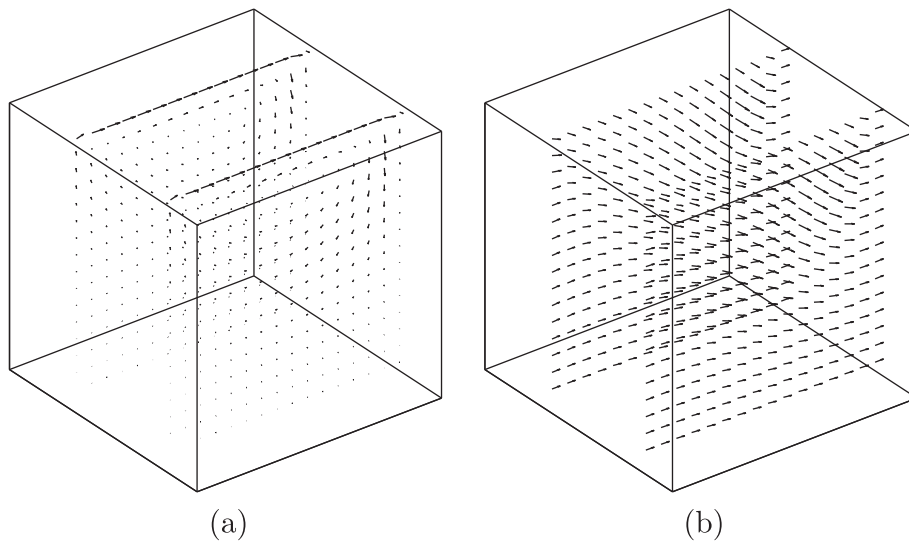

Fig. 5.10. Example 6. Numerical approximations of (a) velocity and (b) normalized magnetic field.
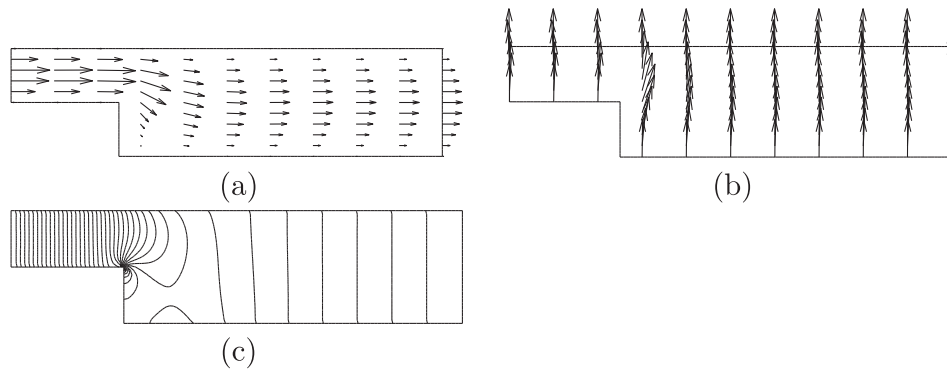
Fig. 5.11. Example 7. Numerical approximations of (a) velocity and (b) normalized magnetic field; (c) pressure contours.
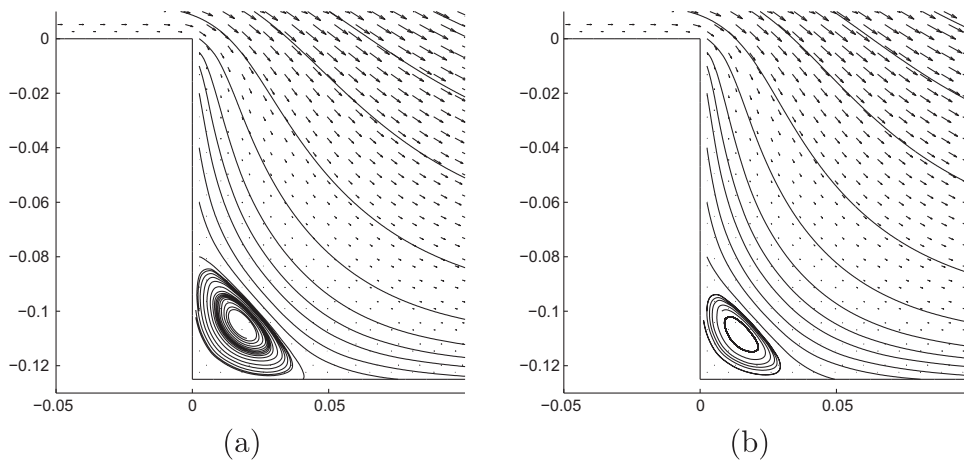

Fig. 5.12. Example 7. Velocity flow vectors and streamlines zoomed in behind the step for (a) κ = 2.5e4 and (b) κ = 1e5.

5.5. Example 7: two-dimensional MHD flow over a step

The example we present here is another classical problem of a flow over a step under a transverse magnetic field; cf. [25]. The magnetic field tends to damp the vortex of the fluid after the step.

The domain is $\Omega = (-0.25, 0.75) \times (-0.125, 0.125) \setminus (-0.25, 0]$ $\times (-0.125, 0]$, with $\Gamma_N = \{(0.75, y): \ y \in (-0.125, 0.125)\}$ and $\Gamma_D = \partial\Omega \setminus \Gamma_N$. We set $\mathbf{f} = \mathbf{g} = \mathbf{0}$, and choose ν = 1e−2, ν_m = 1e5, κ = 2.5e4. The boundary data are given by

$$
\begin{aligned}
\mathbf{u} &= \mathbf{0} & &\text{on } y = 0.125, \{(x,0): x \in (-0.25,0)\} \text{ and } y = -0.125, \\
\mathbf{u} &= \mathbf{0} & &\text{on } \{(0,y): y \in (-0.125,0)\}, \\
\mathbf{u} &= (-25.6y(y-0.125),0) & &\text{on } x = -0.25, \\
(p\underline{\mathbf{I}} - \nu\nabla\mathbf{u})\mathbf{n} &= p_N\mathbf{n} & &\text{on } x = 0.75, \\
\mathbf{n} \times \mathbf{b} &= \mathbf{n} \times \mathbf{b}_D & &\text{on } \partial\Omega, \\
r &= 0 & &\text{on } \partial\Omega,
\end{aligned}
$$

where p_N = 0 and $\mathbf{b}_D$ = (0, 1).

Figs. 5.11 and 5.12 show the solution computed on a mesh with 7168 elements and 43,649 degrees of freedom. It is evident from Fig. 5.11 that the flow field is correctly captured; the magnetic field changes directions due to the coupling effect; the pressure drops behind the step. Fig. 5.12 shows the velocity field in terms of stream lines. The recirculation after the step decreases as the coupling coefficient κ increases. We observe that our numerical method reproduces this damping effect without any oscillation in the numerical solution. The computed solutions agree with the solutions in the literature [14,25].

6. Conclusions

We have introduced a new mixed finite element method for the numerical discretization of a stationary incompressible magneto-hydrodynamics problem, with divergence-conforming BDM elements and curl-conforming Nédélec elements for the velocity and magnetic fields, respectively. The approximation of the velocity field is exactly mass conservative. We have shown the well-posedness of the discrete formulation under a standard small data assumption, and convergence of the approximations under minimal regularity assumptions.

We have proved that the energy norm error is convergent in the mesh size in general Lipschitz polyhedra, and have derived a priori error estimates. As shown in detail in Section 4, in the two-dimensional case there is a loss of $\mathcal{O}(h^\varepsilon)$ in the theoretical error estimates. In the three-dimensional case our error estimates end up falling short by half a power of h for the errors in $\mathbf{u}$ and $\mathbf{b}$, and by a full power in p and r. Nevertheless, the numerical experiments of Section 5 show optimal convergence in all cases. This probably indicates that the sub-optimality is a mere artifact of our technique of proof, which relies on inverse estimates to establish the continuity of the non-linear coupling form. Furthermore, the numerical experiments indicate that the constant C_ε in Theorem 4.3 stays bounded, even though this is not guaranteed by the analysis. Altogether, the computed results are in excellent agreement with results in the literature, and the method correctly resolves the strongest magnetic singularities in non-convex domains. But there is a need to further pursue the theoretical issue of sub-optimal convergence rates.

Based on the theoretical results in [44], we expect the same good performance of our discretization and solution techniques to carry over to the dynamic problem, provided that the non-linear terms are treated (semi) implicitly. We also mention the issue of higher order elements. Here too, we do not expect any deviation from our current computational results. In particular, we expect to see optimal convergence rates for smooth solutions.

The scope of our work can be broadened in a number of additional directions. A very important issue is the investigation of efficient linear solvers for large-scale problems. In such settings iterative solvers are necessary, and this brings up the need for deriving effective and scalable preconditioners. While there are efficient solution techniques for the Navier–Stokes equations as well as for the curl–curl operator, the primary challenge is how to deal with the coupling term, especially when coupling is strong. Preliminary work on this is currently underway.

Another item for future work is the derivation of a non-linear solver that converges more rapidly than the Picard iteration used in our experiments. As we have pointed out in Remark 3.3, developing the Newton iteration for our discretization is somewhat delicate and is subject of ongoing investigation.

References

[1] C. Amrouche, C. Bernardi, M. Dauge, V. Girault, Vector potentials in three-dimensional non-smooth domains, Math. Meth. Appl. Sci. 21 (1998) 823–864.
[2] F. Armero, J.C. Simo, Long-term dissipativity of time-stepping algorithms for an abstract evolution equation with applications to the incompressible MHD and Navier–Stokes equations, Comput. Methods Appl. Mech. Engrg. 131 (1996) 41–90.
[3] D.N. Arnold, An interior penalty finite element method with discontinuous elements, SIAM J. Numer. Anal. 19 (1982) 742–760.
[4] D.N. Arnold, F. Brezzi, B. Cockburn, L.D. Marini, Unified analysis of discontinuous Galerkin methods for elliptic problems, SIAM J. Numer. Anal. 39 (2001) 1749–1779.
[5] A. Bonito, J.-L. Guermond, Approximation of the eigenvalue problem for the time harmonic Maxwell system by continuous Lagrange finite elements, Technical report 2009-121, Institute for Applied Mathematics and Computational Science, Texas A&M University, 2009.
[6] S.C. Brenner, L.R. Scott, The Mathematical Theory of Finite Element Methods, Springer-Verlag, 1994.
[7] F. Brezzi, M. Fortin, Mixed and Hybrid Finite Element Methods, In Springer Series in Computational Mathematics, vol. 15, Springer-Verlag, New York, 1991.
[8] P.G. Ciarlet, The Finite Element Method for Elliptic Problems, North-Holland, Amsterdam, 1978.
[9] B. Cockburn, G. Kanschat, D. Schötzau, Local discontinuous Galerkin methods for the Oseen equations, Math. Comput. 73 (2004) 569–593.
[10] B. Cockburn, G. Kanschat, D. Schötzau, A locally conservative LDG method for the incompressible Navier–Stokes equations, Math. Comput. 74 (2005) 1067–1095.
[11] B. Cockburn, G. Kanschat, D. Schötzau, A note on discontinuous Galerkin divergence-free solutions of the Navier–Stokes equations, J. Sci. Comp. 31 (2007) 61–73.
[12] B. Cockburn, G.E. Karniadakis, C.-W. Shu (Eds.), Discontinuous Galerkin Methods. Theory, Computation and Applications, Lecture Notes in Computer Science Engineering, vol. 11, Springer-Verlag, 2000.
[13] B. Cockburn, C.-W. Shu, Runge–Kutta discontinuous Galerkin methods for convection-dominated problems, J. Sci. Comp. 16 (2001) 173–261.
[14] R. Codina, N.H. Silva, Stabilized finite element approximation of the stationary magneto-hydrodynamics equations, Comput. Mech. 38 (2006) 344–355.
[15] M. Costabel, M. Dauge, Singularities of electromagnetic fields in polyhedral domains, Arch. Ration. Mech. Anal. 151 (2000) 221–276.
[16] M. Costabel, M. Dauge, Weighted regularization of Maxwell equations in polyhedral domains, Numer. Math. 93 (2002) 239–277.
[17] T.G. Cowling, Magnetohydrodynamics, Adam Hilger, England, 1976.
[18] M. Dauge, Stationary Stokes and Navier–Stokes systems on two- or three-dimensional domains with corners. Part I: Linearized equations, SIAM J. Math. Anal. 20 (1989) 74–97.
[19] P.A. Davidson, An Introduction to Magnetohydrodynamics, Cambridge University Press, 2001.
[20] C. Dawson, Foreword for the special issue on discontinuous Galerkin methods, Comput. Methods Appl. Mech. Engrg. 195 (2006) 3.
[21] L. Demkowicz, L. Vardapetyan, Modeling of electromagnetic absorption/scattering problems using hp-adaptive finite elements, Comput. Methods Appl. Mech. Engrg. 152 (1998) 103–124.
[22] M. Discacciati, Numerical approximation of a steady MHD problem, in: U. Langer, M. Discacciati, D.E. Keys, O.B. Widlund, W. Zulehner (Eds.), Domain Decomposition Methods in Science and Engineering XVII, Lecture Notes in Computer Science Engineering, vol. 60, Springer, Verlag, 2008, pp. 313–320.
[23] H.C. Elman, D.J. Silvester, A.J. Wathen, Finite Elements and Fast Iterative Solvers: With Applications in Incompressible Fluid Dynamics, Numerical Mathematics and Scientific Computation, Oxford University Press, 2006.
[24] J.-F. Gerbeau, Problèmes mathématiques et numériques posés par la modélisation de l'électrolyse de l'aluminium, Ph.D. Thesis, École Nationale des Ponts et Chaussées, 1998.
[25] J.-F. Gerbeau, A stabilized finite element method for the incompressible magnetohydrodynamic equations, Numer. Math. 87 (2000) 83–111.
[26] J.-F. Gerbeau, C. Le Bris, T. Lelièvre, Mathematical Methods for the Magnetohydrodynamics of Liquid Metals, Numerical Mathematics and Scientific Computation, Oxford University Press, New York, 2006.
[27] V. Girault, P.A. Raviart, Finite Element Methods for Navier–Stokes Equations, Series in Computational Mathematics, vol. 5, Springer-Verlag, New York, 1986.
[28] V. Girault, B. Rivière, M.F. Wheeler, A discontinuous Galerkin method with nonoverlapping domain decomposition for the Stokes and Navier–Stokes problems, Math. Comput. 74 (2005) 53–84.
[29] J.-L. Guermond, R. Laguerre, J. Léorat, C. Nore, Nonlinear magnetohydrodynamics in axisymmetric heterogeneous domains using a Fourier/finite element technique and an interior penalty method, J. Comput. Phys. 228 (2009) 2739–2757.
[30] J.-L. Guermond, P. Minev, Mixed finite element approximation of an MHD problem involving conducting and insulating regions: the 3D case, Numer. Methods Part. Differ. Eqs. 19 (2003) 709–731.
[31] M.D. Gunzburger, A.J. Meir, J.S. Peterson, On the existence and uniqueness and finite element approximation of solutions of the equations of stationary incompressible magnetohydrodynamics, Math. Comput. 56 (1991) 523–563.
[32] P. Hansbo, M.G. Larson, Discontinuous Galerkin methods for incompressible and nearly incompressible elasticity by Nitsche's method, Comput. Methods Appl. Mech. Engrg. 191 (2002) 1895–1908.
[33] U. Hasler, A. Schneebeli, D. Schötzau, Mixed finite element approximation of incompressible MHD problems based on weighted regularization, Appl. Numer. Math. 51 (2004) 19–45.
[34] R. Hiptmair, Finite elements in computational electromagnetism, Acta Numer. 11 (2002) 237–339.
[35] P. Houston, I. Perugia, D. Schötzau, Mixed discontinuous Galerkin approximation of the Maxwell operator: non-stabilized formulation, J. Sci. Comp. 22 (2005) 315–346.
[36] P. Houston, D. Schötzau, X. Wei, A mixed DG method for linearized incompressible magnetohydrodynamics, J. Sci. Comp. 40 (2009) 281–314.
[37] O.A. Karakashian, W.N. Jureidini, A nonconforming finite element method for the stationary Navier–Stokes equations, SIAM J. Numer. Anal. 35 (1998) 93–120.
[38] O.A. Karakashian, F. Pascal, A posteriori error estimates for a discontinuous Galerkin approximation of second-order elliptic problems, SIAM J. Numer. Anal. 41 (2003) 2374–2399.
[39] P. LeSaint, P.A. Raviart, On a finite element method for solving the neutron transport equation, in: C. de Boor (Ed.), Mathematical Aspects of Finite Elements in Partial Differential Equations, Academic Press, New York, 1974, pp. 89–123.
[40] P. Monk, Finite Element Methods for Maxwell's Equations, Numerical Mathematics and Scientific Computation, Oxford University Press, New York, 2003.
[41] U. Müller, L. Bühler, Magnetofluiddynamics in Channels and Containers, Springer-Verlag, Berlin, 2001.
[42] J.C. Nédélec, Mixed finite elements in $\mathbb{R}^3$, Numer. Math. 50 (1980) 57–81.
[43] A.I. Nesliturk, S.H. Aydin, M. Tezer-Sezgin, Two-level finite element method with a stabilizing subgrid for the incompressible MHD equations, Int. J. Numer. Methods Fluids 58 (2008) 551–572.
[44] A. Prohl, Convergent finite element discretizations of the nonstationary incompressible magnetohydrodynamic system, Math. Model. Numer. Anal. 42 (2008) 1065–1087.
[45] P.H. Roberts, An Introduction to Magnetohydrodynamics, Longman, London, 1967.
[46] D. Schötzau, Mixed finite element methods for incompressible magneto-hydrodynamics, Numer. Math. 96 (2004) 771–800.
[47] D. Schötzau, C. Schwab, A. Toselli, Mixed hp-DGFEM for incompressible flows, SIAM J. Numer. Anal. 40 (2003) 2171–2194.